The Protection of Transmission Lines Connected to DFIG-Based WTGs

by

Xiaoyou Zhang

A thesis
presented to the University of Waterloo
in fulfillment of the
thesis requirement for the degree of
Master of Applied Science
in
Electrical and Computer Engineering

Waterloo, Ontario, Canada, 2021

Author's Declaration

I hereby declare that I am the sole author of this thesis. This is a true copy of the thesis, including any required final revisions, as accepted by my examiners.

I understand that my thesis may be made electronically available to the public.

Abstract

Recently, many countries have proposed various plans to address the issue of climate change, and increasing the capacity of renewables is one of the major common components of such plans. The uncertainty and variability of generation, introduced by renewable energy sources (RESs), pose significant protection challenges to the power systems. Although many studies have identified the challenges associated with the protection of power systems with RESs and have proposed various algorithms to address these challenges, only a few of them comprehensively discuss all the protection challenges within one system. To begin with, a single test system is developed and used to illustrate the protection challenges and to provide a review of the existing protection schemes, which have been proposed in the literature to tackle the protection challenges associated with power systems with RESs.

After introducing the protection challenges associated with the integration of RESs in the power system, this thesis focuses on the protection of transmission lines connected to doubly-fed induction generator (DFIG)-based wind turbine generators (WTGs). DFIG-based WTGs, or namely Type III WTGs, which connect to the power systems via reduced-size converters, raise additional protection challenges such as the maloperation of distance relays due to the frequency deviation of the current measurement caused by the short-circuit characteristics of the DFIGs, and the impact of the fault resistance on the calculated impedance. The protection challenge associated with the frequency deviation caused by the short-circuit characteristics of DFIG is further discussed in detail, and a modified permissive underreaching transfer trip (PUTT) scheme is presented to address the challenge. With the addition of a frequency tracking element, the modified scheme correctly prevents the maloperation of the distance elements during external faults and enables the trip of the relay during internal faults. Besides, the protection challenges associated with conventional distance relays at the terminal of DFIG-based WTGs that are caused by the fault resistance and the frequency deviation associated with the short-circuit characteristics of the DFIG, are addressed and investigated. A modified distance protection scheme is presented to address these protection challenges by using an averaging filter to correct the current phasors and removing the error term caused by the fault resistance in the measured impedance. Pure-fault circuits are used to calculate the pure-impedance of the WTG and pure-fault sequence networks are used to estimate the fault current flowing through the fault resistance. Simulation results show that, for various fault scenarios with different fault resistances, the developed modified distance protection scheme is able to accurately estimate the positive-sequence impedance between the fault and relay location, with fast operations.

Acknowledgements

First and foremost, I sincerely appreciate all the help and guidance offered by my supervisor, Dr. Sahar Pirooz Azad. Dr.Azad’s insight and knowledge steered me through this research. Although it was challenging during the pandemic, she tried her best to support me academically and professionally. I feel truly lucky to have her as my supervisor through my two-year journey as a master's student, and she will always be my role model for the rest of my life and career.

I would also like to express my sincere gratitude to the reviewers, Dr. Mehrdad Kazerani and Dr. Kankar Bhattacharya for their constructive comments to improve this thesis.

Last but not least, I would like to thank my family and my friends for their encouragement and support during my entire study.

Dedication

This thesis is dedicated to my entire family, especially my grandparents, who are always proud of me and supportive of my work no matter what.

Table of Contents

List of Figures

List of Tables

List of Abbreviations

AC: alternating current

CB: circuit breaker

CBR: converter-based resource

CHP: combined heat and power

DC: direct current

DER: distributed energy resource

DFIG: doubly-fed induction generator

DFT: discrete Fourier transform

FCL: fault current limiter

FLISR: fault location isolation and restoration

FRT: fault ride-through

GSC: grid side converter

GW: gigawatts

KCL: Kirchhoff's current law

KVL: Kirchhoff's voltage law

LVRT: low voltage ride-through

MPPT: maximum power point tracking

MW: megawatts

PMU: phasor measurement unit

POTT: permissive overreaching transfer trip

PUTT: permissive underreaching transfer trip

PV: solar photovoltaic

PWM: pulse width modulation

RES: renewable energy source

ROCOF: rate of change of frequency

RSC: rotor side converter

SCIG: squirrel cage induction generator

WTG: wind turbine generator

Chapter 1
Introduction

1.1 Background and Inspiration

With the increasingly severe environmental issues with fossil fuels and the growing energy demand, there is unprecedented interest in renewable energy sources (RESs). The United Nations has listed "affordable and clean energy" as the seventh goal for sustainable development by 2030 [1]. Figure 1.1 shows the global solar and wind power cumulative installed capacity in gigawatts (GW) from 2011 to 2020 [2][3]. A clear upward trend can be noticed even with the global economy shrink during the pandemic in 2020. As a global leader in electricity generation in renewable resources, Canada is also aiming for a goal of achieving 90 percent of domestic electricity coming from non-emitting sources by 2030 [4]. Since only 66.2 percent of electricity came from renewable sources by 2018 [5], a large number of renewable resources are expected to be integrated into the electric grid. For example, the Travers Solar Project with a capacity of 400 megawatts (MW), which will be the largest solar plant in Canada, is expected to commission in 2021 [6]. Besides, the Yarmouth Offshore Wind Farm with a capacity of over 1 GW, which will be the largest wind farm in Canada, is expected to commission in 2025 [7].

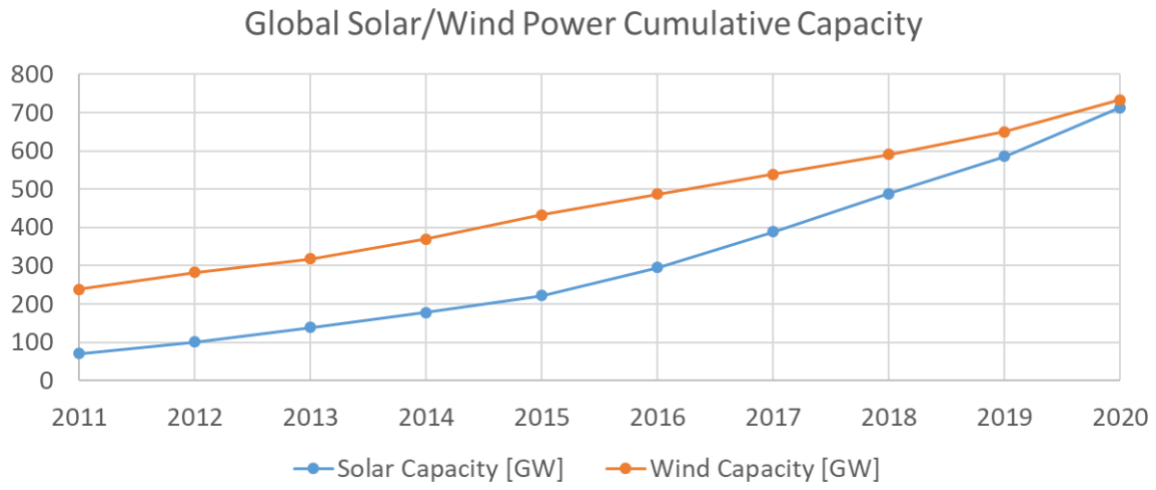

Figure 1.1 Global solar/wind power cumulative capacity [2][3]**.**

Protection challenges associated with the integration of RESs in transmission and distribution systems, are due to the various operation modes of microgrids [8][9], changes in power system

configurations [10], bidirectional current from and to the power systems [9], and various fault current levels seen by relays [11][12]. Besides, many of the RESs, such as solar photovoltaic (PV) systems and wind turbine generators (WTGs), are connected to the grid via converters. To interface with the alternating current (AC) grid, the solar PV systems, which generate direct current (DC) power, require DC/AC converters. Type III and Type IV WTGs are also connected to the grid via back-to-back AC/DC and DC/AC converters to provide independent control of the active and reactive power injection to the grid [13]. The converter-based resources (CBRs) also lead to many protection challenges due to the converter characteristics [9][14][15][16]. Furthermore, for transmission lines connected to Type III WTGs, distance relays may maloperate due to the frequency deviation of the current measurement caused by the short-circuit characteristics of the doubly-fed induction generators (DFIGs) [15], [17]–[22], and impedance error caused by the fault resistance [23][24]. This thesis mainly focuses on the protection challenges associated with a Type III WTG and the details will be explained in the respective chapters.

1.2 Type III WTG

With the decreasing cost and increasing size of large wind turbines, wind farms are widely adopted as major power generation plants by utilities across the world. Due to the large power ratings of wind farms, it is important to address the protection challenges associated with the transmission lines connected to WTGs. Type III WTGs is one of the most widely installed WTGs in power grids due to its variable-speed operation, which is provided by its connection to the grid through converters. Compared to Type IV WTGs with full-sized converters, the main advantage of the Type III WTG is the reduced cost of the converters, especially in large wind farms. This section will provide an introduction to Type III WTGs.

Type III WTGs refer to variable-speed WTGs that are based on DFIGs and are connected to the grid via reduced-sized converters. Figure 1.2 shows the structure of a Type III WTG, where the converters are rated less than the rated power of the entire WTG. The stator of the DFIG injects active power to the grid at rated voltage and rated frequency, while the rotor may inject or absorb active power to or from the grid depending on the operation mode. During the super-synchronous operation mode, the rotor side converter (RSC) injects active power to the grid and during the sub-synchronous operation mode, the RSC absorbs active power from the grid. Since the ratio between the power through the rotor and the power through the stator is approximately equal to the slip ratio [25], for a DFIG with a maximum slip ratio of $\pm 30\%$, the power rating for the converters is 43% of the overall power rating

of the WTG as the ratio between the active power flowing into the rotor and the active power flowing into stator is the slip ratio under a lossless condition [25].

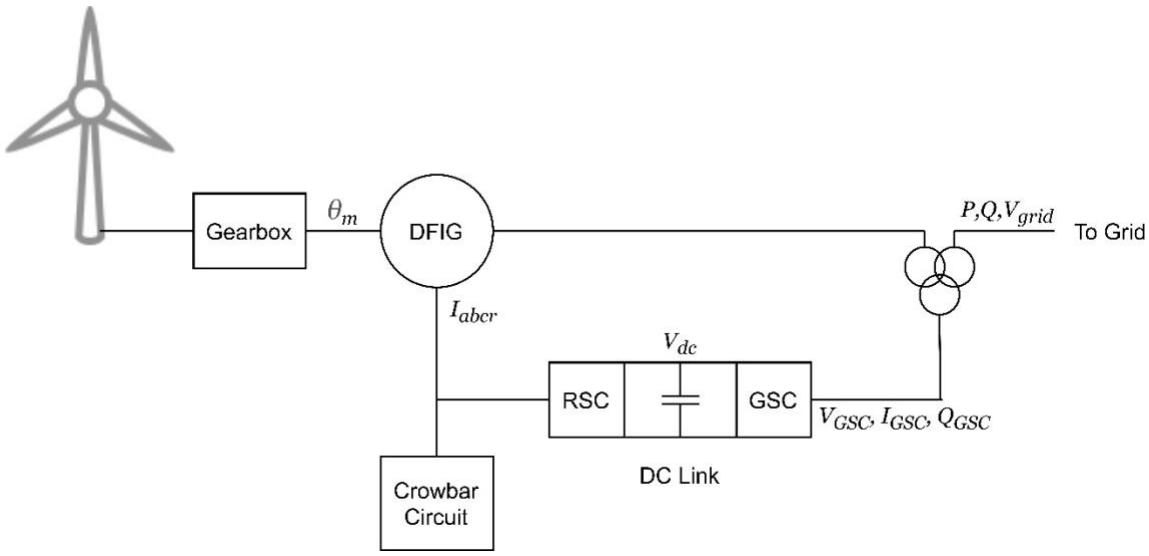

Figure 1.2 Type III WTG.

The converters in a Type III WTG are two-level voltage source converters (VSCs). One of the most commonly adopted strategies for the control of the converters is the vector control method within the d-q frame [25]. Figure 1.3 shows the vector control of the RSC. The maximum power point tracking (MPPT) provides the reference active power P^* based on the mechanical speed of the wind turbine, while the reference reactive power Q^* is selected to provide the desired amount of reactive power to the AC grid. P and Q are the active and reactive power measured at the grid. It is assumed the stator rotating flux is aligned with the air gap flux. Based on the three-phase induced voltage of the stator that is connected to the grid, a phase lock loop (PLL) controller can be used to obtain the angle of the stator flux. The rotor position can be calculated as the integral of the angular speed of the induction machine. By subtracting the rotor position θ_m from stator flux θ_s, the slip angle can be calculated and then used to convert the rotor current from abc frame (I_{abcr}) to dq (I_{dr} and I_{qr}) frame. The voltage references in dq frame (V_{dr}^* and V_{qr}^*) can be subsequently calculated using the voltage drop equations [25]. With the addition of cross-coupling voltages, V_{drcom} and V_{qrcom}, the control signals in the dq frame (V_{dr} and V_{qr}) can be converted back to the abc frame. These voltages are used to generate the pulse width modulation (PWM) signals of the RSC. Figure 1.4 shows the vector control of the grid side converter (GSC). The d-axis component of the grid current (I_{dg}) is controlled to regulate the voltage at the DC

link (V_{dc}) at the reference voltage V_{dc}^{*}. The q-axis component of the grid current (I_{qg}) is controlled by the reactive power measured immediately after the GSC (Q_{GSC}), to regulate the reactive power flow between the GSC and the grid [26]. V_{dgcom} and V_{dgcom} are d-axis and q-axis components of cross-coupling voltages at the grid side.

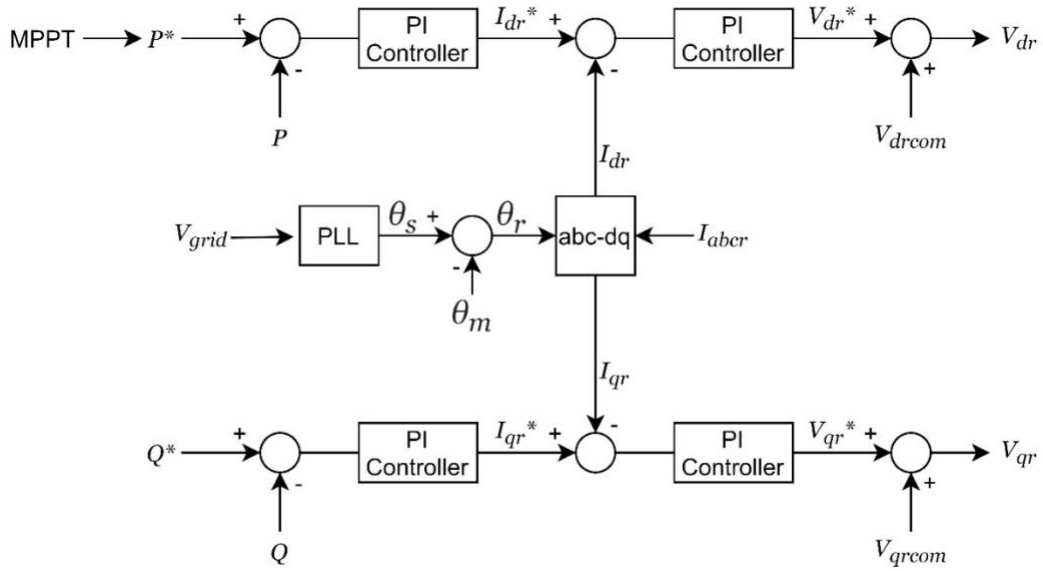

Figure 1.3 The block diagram of the vector control of the RSC.

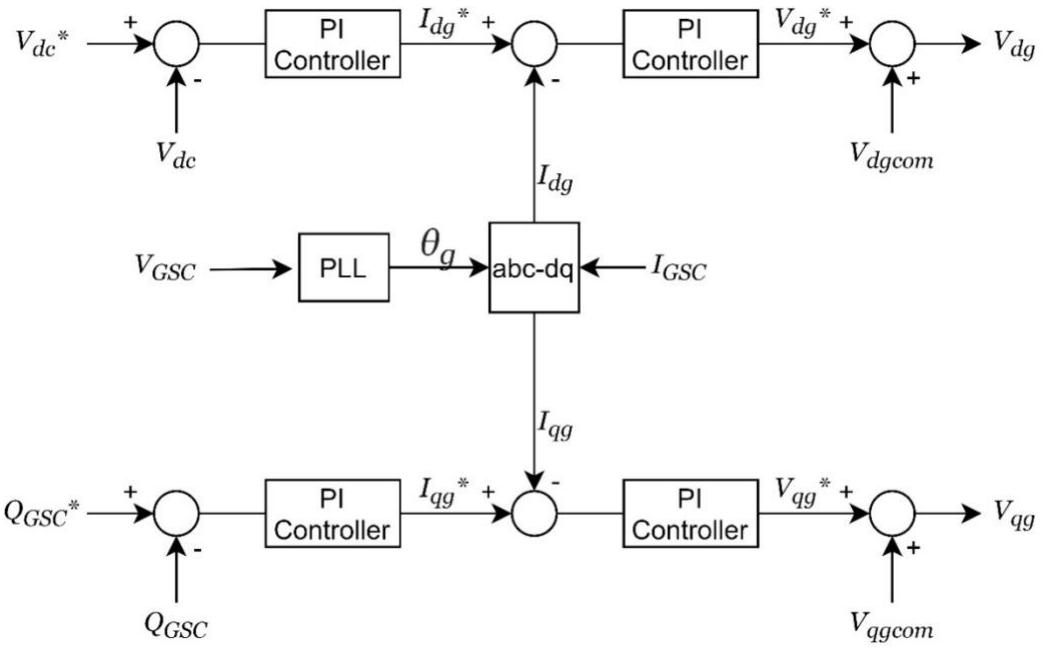

Figure 1.4 The block diagram of the vector control of the GSC.

Several grid codes have specified interconnection requirements for generators. Low voltage ride-through (LVRT) is one of the major requirements to ensure generators remain connected to the grid during temporary faults or disturbances. While different utilities may have slightly different time and voltage requirements [27], one example is shown in Figure 1.5, specified by IEEE standard 1159 [28]. For the area above the curve, a generator should ride through the voltage dips for the associated time duration. As a result, Type III WTGs are required to stay connected to the grid during a voltage dip. During the super-synchronous operation of the DFIG, active power flows from the rotor to the grid. If a fault occurs on the transmission line close to the DFIG, power is transferred to the DC link instead of the AC grid, and thus, large overvoltage may be induced on the DC link. During the sub-synchronous operation of the DFIG, active power flows from the grid to the rotor and then to the stator. If a fault happens on the transmission line close to the DFIG, power is transferred to the rotor but cannot be transferred to the stator as the voltage of the stator collapses, and thus, a large current may be induced at the rotor and stator windings [22]. To prevent such overvoltages and large currents, RSC is disconnected from the rotor by activation of the crowbar circuits, when a fault occurs. The crowbar circuits activation provides a path for the rotor current to flow and dissipate the excess power. Typically, a crowbar circuit consists of a switch and resistor in each phase. The crowbar circuit should be activated when the voltage of the DC link exceeds 1.2 pu, or the rotor current exceeds 2 pu [29], and the duration is typically set between 50 to 100 ms [26]. With the activation of the crowbar, the decline of the short-circuit current is accelerated, while the maximum of the short-circuit current remains unchanged since it solely depends on the highest value of the natural flux, which occurs at the first instant of the voltage dip.

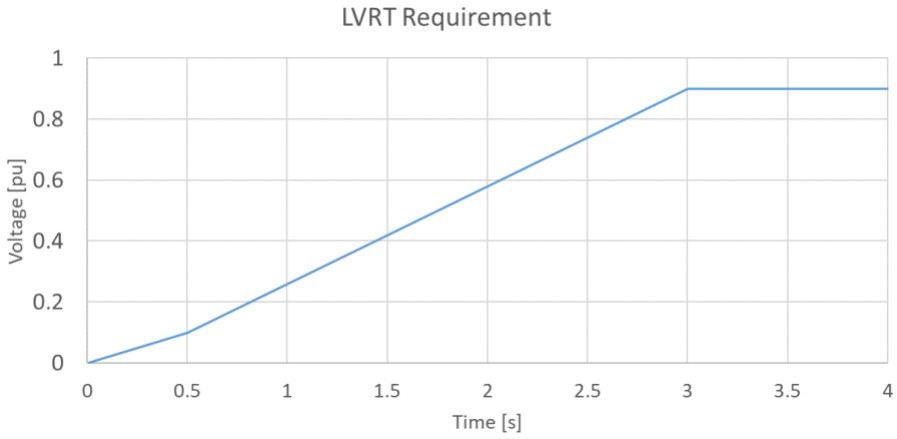

Figure 1.5 LVRT requirement by IEEE 1159.

1.3 Problem Statement and Contributions

The problems that are addressed in this thesis are as follows:

- Although various studies have identified the protection challenges of power systems with RESs and a number of them have proposed protection schemes to overcome the challenges, only a few provide a comprehensive review of all the issues altogether. The lack of a comprehensive test system makes it difficult to extensively understand the various protection challenges of power systems with RESs.
- With the activation of the crowbar circuit, during balanced faults, the dominant frequency of the short-circuit current of DFIGs may significantly deviate from the rated frequency, and thus may affect the performance of various types of relays that rely on phasor calculations, such as distance relays. The calculated fault impedance and the implied distance deviate from the actual distance of the fault to the relay location, resulting in the maloperation of distance relays.
- When the fault resistance is not zero, the measured impedance by a conventional distance relay will be different from the actual impedance. When the transmission line is connected to DFIG-based WTGs, due to the short-circuit characteristics of DFIGs and their fault current frequency deviation, the circuit analysis using phasors calculated by discrete Fourier transform (DFT) can be inaccurate, causing distance relays and other adaptive distance schemes that are based on phasor calculations to maloperate.

The contributions of this thesis are as follows:

- A comprehensive test system is utilized to illustrate the protection challenges of power systems with RESs. The protection challenges result from the various operation modes of microgrids [8][9], changes in power system configurations [10], bidirectional current from and to the power systems [9], and various fault current levels seen by relays [11][12], and converter characteristics when RESs are connected to the power systems via converters [9][14][15][16]. The presented test system is also used to discuss the existing schemes, such as overcurrent-based schemes and directional schemes, which have been developed to overcome the protection challenges.
- A modified permissive underreaching transfer trip (PUTT) is developed to address the protection challenge associated with frequency deviation caused by the short-circuit characteristics of DFIGs. By adding the frequency tracking elements to the conventional PUTT

scheme, the developed scheme is able to provide zonal protection, operates reliably under different operating slips, and requires a low communication bandwidth.

- A modified distance protection scheme is developed to solve the protection challenges associated with conventional distance relays at the terminal of DFIG-based WTGs that are caused by the fault resistance and the frequency deviation associated with the short-circuit characteristics of the DFIG. By using an averaging filter, the phasor correction component is able to correct the current phasors, which are inaccurately calculated using the conventional DFT method. The fault resistance elimination component is able to calculate the actual impedance between the fault and relay location by removing the error term caused by a fault resistance. With the presented modified distance protection scheme, the relay located at the terminal that is close to a Type III WTG is able to correctly identify the fault location and provide zonal protection for transmission lines connected to DFIG-based wind farms.

1.4 Outline

The rest of this thesis is organized as follows:

- In Chapter 2, a comprehensive test system is presented to review the protection challenges of power systems with RESs and existing protection schemes that address these challenges.
- In Chapter 3, the protection challenge associated with frequency deviation caused by the short-circuit characteristics of DFIGs is investigated. A modified PUTT scheme is developed to address this challenge and the performance of the developed protection scheme is evaluated. The developed scheme correctly blocks the maloperation of the distance elements during external faults, enables the trip of the relay during internal faults, and significantly improves the security of the relay at the wind farm side.
- In Chapter 4, the protection challenges associated with conventional distance relays at the terminal of DFIG-based WTGs that are caused by the fault resistance and the frequency deviation associated with the short-circuit characteristics of the DFIG are investigated. A modified distance protection scheme is developed to address these challenges and the performance of the developed protection scheme is evaluated. The developed non-pilot protection scheme is able to accurately estimate the positive-sequence impedance between the fault and relay location, with fast operation.
- Chapter 5 concludes the thesis and provides a summary.

Chapter 2
The Protection of Power Systems with RESs [30]

2.1 Introduction

Over the past decades, power systems with RESs have received large attention due to the increasing electricity demand and severe environmental concerns. The installation of distributed energy resources (DERs) has been proliferated significantly. In the U.S., a 50-52% reduction from 2005 levels in net greenhouse gas pollution is anticipated by 2030, and a goal of 100% carbon pollution-free electricity is set to be reached by 2035 [31]. Although the existing power system market is still dominated by combined heat and power (CHP) generators and other conventional power generators such as diesel, studies have shown that there has been a significant increase in the installed capacity of RESs such as solar PV systems and WTGs, especially in community microgrids, utility microgrids, and remote microgrids [32].

Despite the various advantages of RESs, such as uninterruptible provision of power supply, and peak shaving capability, the protection of power systems with RESs has numerous challenges that must be addressed [8]–[12], [14]–[16], [33]–[36]. These protection challenges are due to the various operation modes of microgrids, changes in power system configurations, bidirectional current from and to the power systems, and various fault current levels seen by relays. Furthermore, the fault current characteristics of converters add more challenges to the protection of power systems with RESs that are connected to the power grid via converters. Various studies have identified these challenges and a number of them have proposed protection schemes to overcome the challenges [37]–[44]. Among these studies, only a few provide a comprehensive review of the issues altogether. For example, [36] includes six different test systems to study the fault identification challenge associated with fault current characteristics and the possible solutions. Also, [9], [14], and [33] include more than three test systems to discuss the challenges of microgrids with RESs from different viewpoints. Besides, the proposed protection schemes which address one or more protection challenges of the microgrids with RESs, such as [37]–[40], discuss and simulate their schemes based on different test systems as well.

The lack of a comprehensive test system makes it difficult to extensively understand the various protection challenges of power systems with RESs. Thus, section 2.2 presents a single comprehensive test system, which is utilized, in section 2.3, to illustrate all the protection challenges due to the various operation modes of microgrids, changes in power system configurations, bidirectional current flow,

various fault current levels seen by relays, and converter characteristics. In section 2.4, the presented test system is used to discuss the existing schemes, such as overcurrent-based schemes and directional schemes, which have been developed to overcome the protection challenges.

2.2 The Comprehensive Test System

Figure 2.1 shows the comprehensive test system, which is based on the conventional IEEE 13-bus system [45]. In this presented system, buses 675, 692, and 652 are modified with the addition of loads and DERs. Switch SW1 is added between buses 646 and 611 so that a looped system is formed once the switch is closed. Once there is a power outage between buses 611 and 671, the connection between buses 646 and 611 can provide an alternate path to restore the power supply to buses 684 and 652. Circuit breakers (CBs), which are controlled by their corresponding relays and are connected to the DER-buses are also shown in this figure. Two islanded microgrids can be formed once CB2 and CB4 are open, and the rest of the system is considered as the main grid. Six short-circuit fault scenarios F1-F6 are considered in this section.

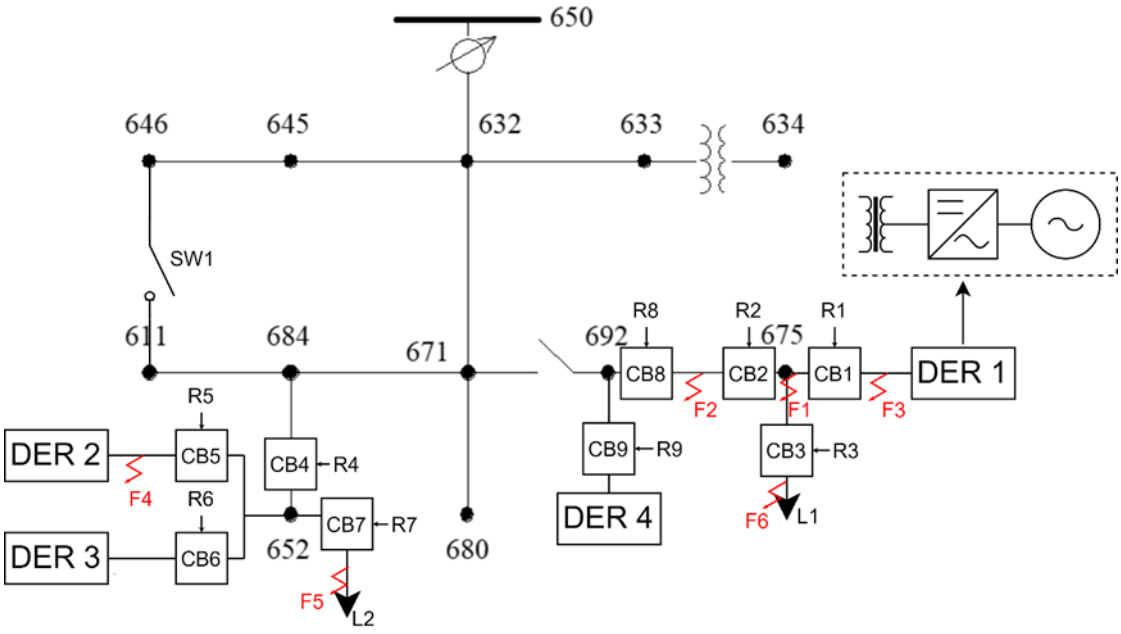

Figure 2.1 The comprehensive test system.

2.3 Protection Challenges of Power Systems with RESs [8]–[12], [14]–[16], [33]–[36]

This section will provide a comprehensive discussion about the protection challenges of power systems with RESs using the developed test system. The discussion will focus on the protection challenges of buses 675 and 652, which are connected to one or multiple DERs. As shown in Figure 2.1, bus 675 is connected to a converter-based DER (DER 1) and bus 652 is connected to two general-type DERs (DER2 and DER3). In this section, DER 4 is assumed to be disconnected from the system. The challenges of various operation modes of microgrids, changes in power system configurations, bidirectional current from and to the power systems and various fault current levels seen by the relays, will be discussed in sections 2.3.1 – 2.3.4. Then, section 2.3.5 will discuss the converter fault current characteristics that further complicate the protection of power systems with CBRs.

2.3.1 Various Operation Modes of Microgrids [8][9]

There are two main operation modes of microgrids, namely grid-connected and islanded. For example, in Figure 2.1, the microgrid consisting of DER2, DER3, and L2 operates in the grid-connected mode when CB4 is closed; however, when CB4 is open, this microgrid is disconnected from the grid and operates in the islanded mode. The microgrid protection schemes should operate properly during both operation modes and the transition between them. Under the grid-connected mode, the protection system of the microgrid should be properly coordinated with that of the main grid. Considering the large current fed from the grid, the overcurrent settings of the relays in the grid-connected mode are different from those under the islanded mode, where the fault current is much smaller. Besides, without proper protection schemes, the transition from the grid-connected mode to the islanded mode, so-called islanding, may result in off-nominal frequency and inaccurate voltage measurements, and may further prevent the re-connection and re-synchronization of the microgrid.

2.3.2 Power System Configuration [10]

In the conventional IEEE 13-bus system, switch SW1 is open, and the test system is radial. In this radial system, the protection relays are coordinated by considering the upstream relay as the backup relay for the downstream relays. For example, with SW1 open, buses 611 and 652 are supplied through bus 684, and therefore the overcurrent relay at bus 684 should operate slower than the overcurrent relays at buses 611 and 652. However, once there is a power outage between buses 684 and 671, SW1 should close, so that buses 684 and 652 are supplied through bus 611, and thus the original coordination between

relays at buses 611 and 684 will be lost. In this configuration, the overcurrent relay at bus 684 should operate faster than the overcurrent relay at bus 611, and the relay at bus 652 should operate faster than the relay at bus 684. To overcome the protection challenges due to the power system configuration, the relay settings are required to change adaptively with the changes in the system configurations and power flow directions [10].

2.3.3 Bidirectional Current Flow [9]

Another major protection challenge in the power systems with DERs is due to the bidirectional current flow. In the test system shown in Figure 2.1, during the grid-connected mode of operation, three power flow scenarios are possible: (a) The DER is turned off, and the load is fully supplied from the main grid, and thus the power flows from the grid to the load; (b) The DER is turned on, and the load is supplied by both the main grid and the DER; (c) The DER generates more power than the load, and the DER feeds the grid (assuming back-feeding is enabled). Under the islanded mode of operation, the DER fully supplies the load. The four aforementioned possible power flow scenarios are illustrated in Figure 2.2. Three possible power flow scenarios under faults F1-F3 are shown in Figure 2.3. It can be observed that the power flow directions under some faults may resemble those under the normal condition, and in such scenarios, the relays might malfunction. For example, under F2, as shown in Figure 2.3(b), when there is a fault on the grid, DER 1 feeds both the load and the grid, and this scenario resembles scenario (c) of Figure 2.2 where there is no fault in the system. As a result, during the normal condition when DER1 generates a considerable amount of power, R2 may see a large current, comparable to the fault current and may detect a fault. Similarly, fault F1 shown in Figure 2.3(a) may resemble scenario (b) of Figure 2.2, and relays R1-R3 may malfunction under normal or fault conditions if they are not properly tuned.

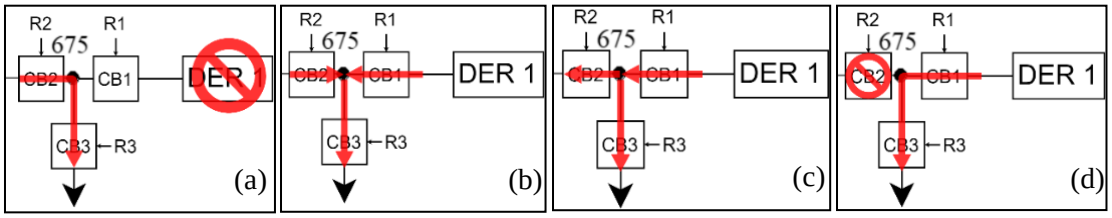

Figure 2.2 Possible power flow directions under the normal condition.

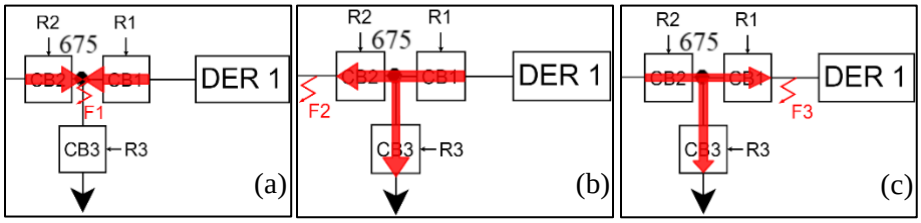

Figure 2.3 Possible power flow directions under faults F1, F2, and F3.

Furthermore, fault detection becomes even more complicated once there are multiple DERs connected to the same bus. Taking bus 652 as an example, a bus fault at bus 652 has to be isolated from all sources including DER2, DER3, and the main grid. Assuming that the two DERs are initially turned off and are not supplying any current to the system, R5 and R6 will not send a trip signal to CB5 and CB6 during a fault at bus 652. However, once any of the DERs are turned on before the fault is removed, bus 652 will be energized. Thus, in the event of a bus fault, it is desired to lock out the connected DERs to avoid unexpected energization [9].

Another fault scenario is shown in Figure 2.4, where the overcurrent relay R5, without a directional element, may malfunction [9]. Assuming bus 652 is isolated from the grid, ideally, CB5 should trip for F4, but not for F5. Under F4, R5 sees a fault current I fed by DER3. Under F5, R5 sees a fault current I' fed by DER2. Assuming DER2 and DER3 are identical, $|I|$ will be equal to $|I'|$ but will be in the opposite direction. Since R5 is an overcurrent relay that does not include any directional element, it cannot distinguish F4 from F5. Therefore, R5 may send the wrong trip signal to CB5 for a fault F5. The same may happen to R6. Thus, a directional element is suggested to be added to the overcurrent relays to overcome this protection challenge. However, this is not the ultimate solution as the performance of directional relays can be affected by converters, which will be discussed in section 2.3.5.

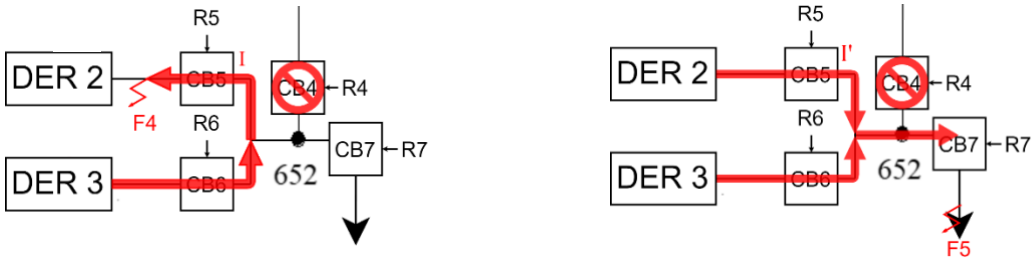

Figure 2.4 Bus 652 with multiple DERs.

2.3.4 Various Fault Current Levels [11][12]

In a power system, the current magnitude may also increase or decrease with the addition of DERs to the grid [11]. Under different microgrid operation modes and different operation statuses of the DERs, the fault current level may vary at a certain location. Since the existing protection systems for distribution grids are mostly designed based on the assumption that power only flows from the grid towards the load and are based on overcurrent relays set at fixed current levels, they may malfunction with the addition of new DERs to the power system, and the coordination between relays may be lost [12]. For example, at bus 652, the fault current seen by R7 under F5 may have five different levels based on the microgrid operation modes and the connection status of the DERs, when (a) both DERs operate in the grid-connected mode; (b) only one of the DERs operate in the grid-connected mode; (c) the microgrid operates in the grid-connected mode and both DERs are turned off; (d) both DERs operate in the islanded mode; (e) one of the DERs operates in the islanded mode. As a result, R7 should be properly set up so that it can selectively identify fault events under all these scenarios, and backup relays R4-R6 should be coordinated accordingly with R7.

2.3.5 Converter Characteristics [9][14][15][16]

A large number of DERs are connected to the grid via converters. An example of such CBRs is DER1, which is represented with a source behind a converter (and a transformer upon necessity), as shown in Figure 2.1.

Due to the non-linear characteristics of converters, various challenges are introduced to the protection system by CBRs due to their complex short-circuit behavior, limited converter current, inaccurate sequence impedance model, and low inertia [14][15]. These protection challenges are not only limited to microgrids. They may exist in any electric grid with integrated CBRs.

- The short-circuit behavior of CBRs depends on the converter control scheme such as droop control and PQ control [15], and the operation mode of the CBRs such as the sub-synchronous or super-synchronous operation of Type III and IV WTGs [16]. Depending on the control scheme and the operation mode, when there is a sudden change in the voltage and current under fault events, transients with off-nominal frequencies are introduced to the system along with phase shifts. As the current frequencies deviate from the rated frequency, the measurement errors will cause relays to malfunction. When the current frequency is significantly different

from the voltage frequency, the phasor forms of voltage and current and any related calculations will be erroneous [16].

- The internal protection system of converters limits the current within a certain level, even under faults. Thus, overcurrent-based schemes may malfunction as the limited fault current may not reach the trip setting of the relays. Besides, most converters are designed without the ability to provide a negative-sequence current component. Thus, negative-sequence relays, which are used for detecting unbalanced faults, can no longer function properly in power systems with CBRs.

- Converters with fault ride-through (FRT) capability are controlled such that they remain connected to the grid during faults and provide reactive power support to the grid. Therefore, they should be modeled as current sources rather than voltage sources during fault studies [9]. The current sources are equivalent to either a constant voltage source along with a variable impedance or a variable voltage source with a constant impedance. However, in conventional analysis of CBRs during faults using symmetrical components, the voltage source magnitude and impedance representing CBRs are assumed to be constant. Hence, the corresponding calculations are inaccurate.

- Power systems with CBRs have much lower inertia compared to those with synchronous generators, resulting in a higher rate of change of frequency (ROCOF) [9][14]. Due to the high ROCOF, the addition or loss of a large load or CBR due to faults will quickly cause a significant change in the frequency and might destabilize the power system. Thus, the protection system of such power systems should operate fast enough to detect and isolate faults to arrest the frequency changes to avoid cascading generation loss and ensure stable recovery of power systems. Also, the relay settings need to be adjusted so that CBRs can tolerate higher ROCOF without being unnecessarily tripped offline. Besides, the conventional overcurrent relays may not be able to track large frequency decays, and may maloperate or lose coordination with other relays.

2.4 Existing Protection Schemes

This section addresses various types of recently proposed relays to solve the aforementioned challenges. The schemes based on overcurrent-relays can solve the challenges of various fault current levels and various operation modes of the microgrid [37]–[39]. The schemes based on directional relays can solve

the challenge associated with bidirectional current flow [40]–[42]. Other protection methods such as differential relays [36], setting-less schemes [43], and communication based-schemes and intelligent schemes [44] are also proposed to solve the challenges.

2.4.1 Overcurrent-Based Schemes

Due to the fault current characteristics of power systems with CBRs, as discussed in section 2.3, the conventional overcurrent protection devices such as overcurrent relays may malfunction and lose coordination with downstream relays. Two of the most widely proposed solutions to overcome the malfunctioning of overcurrent devices are fault current limiters (FCLs) and adaptive protection schemes.

To resolve the challenge of various fault current levels, FCLs are inserted between the DERs and buses to limit the fault current level. With the insertion of FCLs into the power system, the fault current can be limited to a level comparable to that of the original grid where there are no DERs [37]. By limiting the fault current levels, the coordination between the overcurrent devices can be restored. As an example, in Figure 2.1, assume R8 and R3 are coordinated before DER1 and DER4 are installed: When DER4 is added to the system, it will increase the fault current level at buses 675 under F6, and R8, as an upstream backup relay, may trip faster than R3, and thus the coordination between R8 and R3 will be lost. The addition of an FCL between bus 692 and DER4 limits and restores the fault current level and trip time approximately to the scenario where DER4 is disconnected from the grid, thus restoring the coordination between R3 and R8. While the major advantage of FCLs is to restore the coordination of overcurrent protection devices by reducing the level of fault current, FCLs may lead to the maloperation of other overcurrent relays. In the previous example, due to the FCL between DER4 and bus 692, the fault current detected by R9 is reduced and therefore, the performance of R9 is negatively affected.

Some alternate solutions, namely adaptive schemes, are proposed to solve the challenges of various operation modes and various fault current levels of power systems. [38] proposes an adaptive scheme that identifies the operation mode of the microgrid, based on the measurement data from relays located at the main grid and the DERs, and calculates the time dial settings for the overcurrent relays at every sampling instant. One major requirement to achieve reliable performance in this method is a high communication capacity among relays at different locations. [39] proposes another adaptive scheme that identifies the operation mode of the microgrid based on the zero-sequence impedance angle, and uses specific fault detection schemes under each operation mode. Under the islanded mode, since the

overcurrent devices are more adversely affected due to the significantly smaller fault current level, voltage dip is used for fault detection, but the conventional overcurrent relays are still used under the grid-connected mode. While this scheme overcomes the challenge associated with various operation modes, it fails to resolve the various fault current levels challenge. For example, in Figure 2.1, assuming the system is properly grounded, the equivalent zero-sequence impedance angles seen by R7 are different under grid-connected and islanded operation modes of the microgrid. The real-time zero-sequence impedance angle detected by R7 is compared with these expected angles to identify the real-time operation mode of the microgrid, and to choose the fault detection scheme accordingly. However, according to section 2.3.4, the fault current still varies under the grid-connected operation mode and the conventional overcurrent relays may malfunction.

2.4.2 Directional Schemes

Directional relays can detect the direction of current and power flow based on the torque caused by the angle difference between the measured current and voltage. The directional relays can be respectively categorized into positive-sequence relays for symmetrical fault detection, negative-sequence relays for asymmetrical fault detection, and ground relays for ground fault detection. For all three types, the torque depends on the magnitude and the phase angle of the measured voltage, measured current, and the sequence/phase impedance of DERs. Although directional relays can address some of the aforementioned challenges such as bidirectional current flow in power systems [9], they may maloperate due to incorrect calculations of torque in power systems with CBRs.

One of the issues is caused by the inaccurate modeling of the symmetrical components of CBRs [35] [40]. This problem can be solved by accurate modeling of the sequence impedance of the CBRs [40]. The idea of superimposed impedance is proposed to correctly evaluate the equivalent impedance of CBRs, using the memorized values of current and voltage measurements from the most recent cycle [40]. While the superimposed impedance significantly improves the accuracy of conventional directional relays, it can still be affected by the control scheme of the CBRs, fault conditions, and load current. When the frequency is not high enough, the influence of the inductive and capacitive components in the circuit and the control system with high-bandwidth current loops on the superimposed impedance can not be neglected [34]. As a result, it is proposed that the high-frequency impedance of DERs should be used in combination with the superimposed impedance for fault detection in power systems with CBRs [41]. The high frequency refers to the increase in the transient

frequency when there is a sudden voltage drop during the fault. However, to calculate the high-frequency impedance, a high sampling rate is required for the relay, leading to an increased cost.

The maloperation of directional relays may also be caused by the phase and frequency deviation between the fault voltage and current measurements [16]. A modified load encroachment function is proposed in [42] to supervise the directional relays to prevent relay maloperation by ensuring all normal load conditions are excluded from the relay trip zone. The load encroachment zone is set up to block the relay from operating during large loads. To accommodate for the phase and frequency deviation, the modified load encroachment zone is phase-shifted, according to the phase shift of the fault current and voltage so that it can correctly block the maloperation of the directional relays.

2.4.3 Other Schemes

In addition to the aforementioned relays, other protection devices and schemes have been proposed for the protection of power systems with CBRs [14][36][43][44]. Differential relays provide reliable protection in power systems as they are based on Kirchhoff's current law (KCL) in the protection zone. However, the bidirectional current in power systems may complicate the settings of such relays [36]. This issue can be avoided using setting-less protection schemes [43]. In a setting-less scheme, a fault is detected if any of the physical and electrical laws such as KCL, Kirchhoff's voltage law (KVL), Ohm’s law, or heat transfer laws, are violated while system states are dynamically estimated from measured data. Relays based on traveling waves are also proposed for power system protection [14]. While the traveling-wave-based scheme is theoretically immune to the aforementioned challenges, it has not yet been tested in real-world power systems and requires further evaluation.

In addition to the aforementioned schemes, with the development of smart grid technologies, fast communication systems and phasor measurement units (PMUs), distance relays [8] and communication-based schemes such as pilot protection schemes, fault location isolation and restoration (FLISR) schemes [14], and schemes based on data mining [44] are proposed as alternate options to protect the power systems. Although distance relays are not widely adopted due to the small impedances of microgrids, they can help protect high-cost transformers in industrial power systems [14], and supervise pilot protection schemes that are favored for their fast operation. FLISR schemes are useful for power systems with complex distribution and heavily depend on communication due to the ability to share information among protective devices [14]. The data-mining-based scheme uses the random forest tree technique as the classifier and a learning-from-data approach to classify the features of the acquired dataset from the relays and determine if any fault has occurred [44]. While the communication-

based schemes are able to address almost all the aforementioned challenges with significant accuracy and reliable performance, communication bandwidth and cyber-security are critical concerns that require attention as well.

2.5 Conclusions

This chapter presented a single comprehensive test system based on the IEEE 13-bus system [45] with renewable DERs, which can be used to study all the protection challenges associated with power systems with RESs. Although various studies have identified these challenges [8]–[12], [14]–[16], [33]–[36] and a number of them have proposed protection schemes to overcome the challenges [37]–[44], only a few provide a comprehensive review of the issues altogether. The lack of a comprehensive test system makes it difficult to extensively understand the various protection challenges of power systems with RESs. This chapter comprehensively reviewed the protection challenges of RES-connected power systems and the existing protection schemes that are already proposed to address the challenges, using the developed test system. The addressed protection challenges are associated with the various operation modes of microgrids, changes in power system configurations, bidirectional current flow, various fault current levels seen by relays, and the converters' fault current characteristics. The reviewed protection schemes include overcurrent-based, directional, differential, setting-less, traveling-wave-based, distance-based, communication-based, and data mining. So far, the communication-less schemes are not able to solve all the protection challenges of power systems with RESs, while the communication-based schemes require high communication bandwidth and have to deal with cyber-security concerns. It can be concluded that there are trade-offs among the performance, the complexity, and the cost of the proposed protection schemes, and a comprehensive protection scheme that solves all the challenges is in great demand.

Chapter 3
Modified PUTT Scheme [46]

3.1 Introduction

With the development of wind energy technologies and the reduced average cost associated with larger wind turbines, large on-land and off-shore wind farms are connected to the power grid [13]. DFIGs are among the most widely installed wind farms due to the various advantages that they offer such as variable speed operation, high power conversion efficiency, and improved power quality [13]. In order to increase the reliability and stability of the power grid, wind farms are required to be equipped with the FRT capability. In DFIG-based wind farms, to provide FRT capability and prevent damages to the machine-side converters, crowbar and chopper circuits are used [17]. With the activation of crowbar circuits, DFIGs present the same short-circuit characteristics as the squirrel cage induction generators (SCIGs), but with a much wider slip range [17]. The short-circuit behavior of DFIGs is comprehensively studied in [15], [17]–[22]. During balanced faults, the dominant frequency of the short-circuit fault current of DFIGs may significantly deviate from the rated frequency, and thus may affect the performance of various types of relays that rely on phasor calculations, such as distance relays. Distance relays are among the most popular relay types for the protection of long transmission lines and form a major element in pilot protection schemes. A distance element measures the impedance between the relay and the fault location using the phasors of voltage and current measurements [23]. Due to the DFIGs' short-circuit behavior [15], [17]–[22], the phasors of current deviate from their actual values. Consequently, the calculated fault impedance and the implied distance deviate from the actual distance of the fault to the relay location, resulting in the maloperation of the distance relays [21].

To address the protection challenges associated with the distance relays on transmission lines connecting DFIG-based wind farms, several innovative protection schemes are proposed [18]–[24], [35]. In [49], the zone settings of distance elements are calculated adaptively to accommodate the slip change of the DFIG. However, this method is only applicable assuming that the slip is known and the slip does not change at the instant when the fault occurs. In [21], [47], and [48], time-domain calculations are adopted in place of phasor calculations to determine the location of the fault. The inductance and resistance of the line are estimated using the least-square method and the relationship between the instantaneous voltage and current. In [52], the structural similarity between the measured

fault current at the wind farm side and the grid side is calculated to distinguish internal faults from external faults. The drawbacks of [21], [47], [48], and [52] are associated with the computation bandwidth and memory requirements to perform the necessary calculations. Besides, in [50], the fault direction is determined by measuring the phase angle shift and amplitude damping of the fault current. In [51], a modified permissive overreaching transfer trip (POTT) scheme, in addition to the overreaching elements in the conventional POTT scheme, determines the fault direction by comparing the peak-to-peak values between the detected fault current waveform with the expected fault current waveform of the DFIG. However, [50] and [51] are only capable of detecting forward or backward faults and lack the ability to provide zonal protection.

In this thesis, a new relaying scheme is developed to address the protection challenge associated with frequency deviation caused by the short-circuit characteristics of DFIG. This new relaying scheme is inspired by the protection scheme proposed in [54], where the fault location is determined by a modified distance protection scheme, that uses the frequency deviation detected by the relays located at both ends of the protected line. In [54], during a reverse fault, relays at both terminals of the transmission line detect the rated frequency since the short-circuit current is fed from the AC grid. During an internal fault, since the DFIG side relay detects a fault current fed from the DFIG while the grid side relay detects a fault current fed from the AC grid, under large slip values, the DFIG-side relay detects a large frequency deviation while the grid side relay detects the rated frequency. During an external fault, since both relays detect a fault current fed from the DFIG, under large slip values, both relays will detect a large frequency deviation. Based on the frequency deviation and the fault current characteristics, [54] determines the location of the fault with respect to the protection zones of the relay and provides backup protection for adjacent lines.

This chapter presents a modified PUTT scheme based on the detection of the frequency deviation measured by the relays at the two ends of the line, which uses a less complex algorithm compared to [54], to improve the reliability and simplicity of the protection scheme.

3.2 Test System

The test system used in the studies of this chapter is shown in Figure 3.1. A DFIG-based wind farm is connected to the AC grid through two segments of 100 km transmission lines. Relay W and Relay M are located at the DFIG side and the grid side of the protected segment of the transmission line, respectively. The underreaching elements of both relays cover 80% of the protected line (Zone 1) and

the overreaching element of relay W covers 140% of the protected line (Zone 2). The presented modified PUTT scheme is applied to Relay W. The parameters of the system are provided in Table 3.1. The faults studied in this chapter occur at $t = 15.5\ s$ and are cleared at $t = 16\ s$.

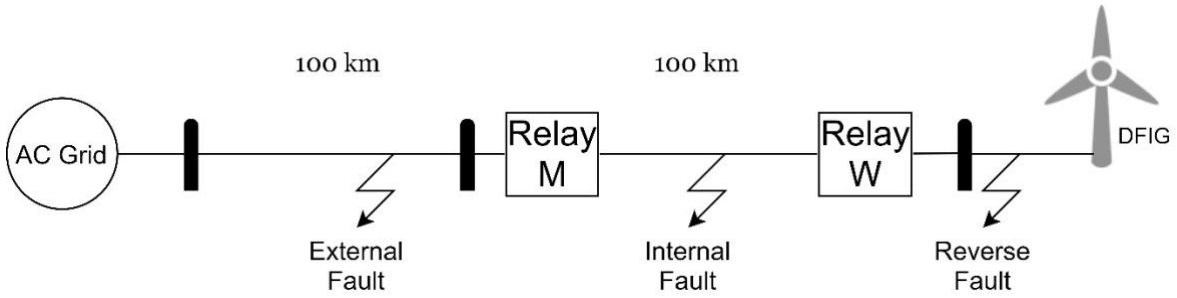

Figure 3.1 Test system for transmission lines connecting DFIG.

Table 3.1 Parameters of the DFIG test system

Component	Parameter	Value
DFIG	Rated power	5 kVA
	Rated voltage	0.69 kV
	Rated frequency	60 Hz
	Stator resistance	0.0054 pu
	Rotor resistance	0.00607 pu
	Stator inductance	0.1 pu
	Rotor inductance	0.11 pu
	Slip range	+/- 30%
DFIG-based Wind Farm	Rated power	50 kVA
	Rated voltage	33 kV
AC Grid	Rated voltage	132 kV
	Rated frequency	60 Hz
Transmission Lines	Positive-/negative-sequence impedance	$0.1\angle 87°$ pu / 100 km
	Zero-sequence impedance	$0.37\angle 73°$ pu / 100 km

3.3 Problem Statement

Conventional distance relays measure the positive-sequence impedance between the fault and relay location to locate the fault. Assuming a short-circuit fault, the measured voltage at the relay location

equals the total voltage drop between the relay and the fault location. For inter-phase faults, the positive-sequence impedance is calculated by

$$Z_{1f} = \frac{V_1 - V_2}{I_1 - I_2} = \frac{V_a - V_b}{I_a - I_b}, \tag{3.1}$$

where V_1, V_2, and I_1, I_2 denote the positive- and negative-sequence voltages and currents, and V_a, V_b, and I_a, I_b denote the phase A and phase B voltages and currents. For single-phase faults, the positive-sequence impedance is calculated by

$$Z_{1f} = \frac{V_a}{I_a + I_0 \frac{Z_0 - Z_1}{Z_1}}, \tag{3.2}$$

where Z_0 and Z_1 denote zero-sequence and positive-sequence impedance of the entire protected line, I_0 denotes the zero-sequence current, and Z_{1f} denotes the calculated positive-sequence impedance between the fault location and relay.

As shown in (3.1) and (3.2), in distance relays, current and voltage phasors are used to calculate the positive-sequence impedance between the fault and relay location. Typically, phasors are calculated based on the assumption that the frequency of the measured signals is the rated frequency, which is a valid assumption for synchronous generators. However, for DFIG-based generators, due to a larger operating slip range, the frequency of the short-circuit current may significantly deviate from the rated value. Consequently, the calculated phasors under the deviated frequency are inaccurate and deviate from the actual value, and as a result, the impedance calculated using (3.1) or (3.2) becomes incorrect and causes conventional distance relays to mal-function.

In this section, the protection challenges associated with the frequency deviation of the fault current caused by the short-circuit behavior of the DFIG during balanced and unbalanced faults are discussed. Furthermore, the performance of the conventional PUTT scheme, which uses distance elements and is implemented in the wind farm side relay, is evaluated.

3.3.1 Balanced Faults

In order to protect the rotor side converter and to provide the FRT capability, the rotor side converter is disconnected from the rotor during a fault to avoid a large current in the rotor circuit, and the rotor is then connected to a crowbar circuit. As the rotor is shorted through the crowbar circuit, the DFIG operates as a SCIG [18]. As a result, the short-circuit behavior of DFIG-based wind turbines resembles

SCIG's fault response, when the crowbar circuit is activated [18]. Thus, for DFIG-based wind turbines, during crowbar activation, the balanced fault current can be expressed as

$$i(t) = \frac{V_{max}}{1-s}\left(\frac{1}{X'} - \frac{1}{X_{\sigma s} + 1.5X_{ms}}\right)e^{-\frac{t}{T'}}\cos\big((1-s)\omega_1 t + \theta\big) + \frac{V_{max}}{1-s}\left(\frac{1}{X'}e^{-\frac{t}{T_a}}\cos(\theta)\right), \qquad (3.3)$$

where V_{max} is the magnitude of the generated source voltage; s and ω_1 are the slip and the fundamental frequency of the DFIG; X', $X_{\sigma s}$, X_{ms} are the circuit parameters; θ is the fault inception angle (phase shift due to the fault); and T_a and T' are the time constants of the stator and fault current transients of the rotor, respectively [22]. As shown in (3.3), in DFIGs, the frequency of the fault current is $(1-s)\omega_1$, and there is a phase shift θ in the fault current. Since the relays are conventionally set up to calculate the current phasor at the nominal frequency ω_1, without considering any phase shift, the change in the frequency and phase shift will result in an inaccurate current phasor calculation and consequently the maloperation of the distance elements of the relays located close to the DFIG. Under small slip values, the DFIG operates as a fixed-speed generator similar to a SCIG. Therefore, the frequency deviation is negligible and the performance of the distance elements is not affected. However, under large slips, the resulting frequency deviation of $(1-s)\omega_1$ may affect the performance of distance elements. With the nominal frequency of 60 Hz and a slip range of -30% to $+30\%$, the fault current of a DFIG can contain frequencies from 42 Hz to 78 Hz. Figure 3.2 shows the fault current measured by Relay W under an internal balanced fault for synchronous ($s = 0$), super-synchronous ($s = -30\%$) and sub-synchronous ($s = +30\%$) operations of the DFIG. It can be seen that, as expected, the dominant frequency of the short-circuit current is equal to $(1-s)\omega_1$, and for large slip values, the dominant frequency of the current significantly deviates from the rated frequency.

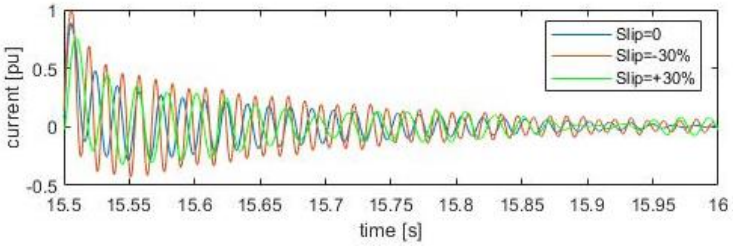

(a) Time domain

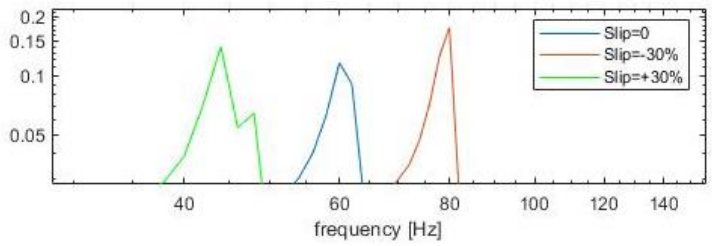

(b) Frequency domain

Figure 3.2 Phase-A current at Relay W after an internal balanced fault for synchronous ($s = 0$), super-synchronous ($s = -30\%$) and sub-synchronous ($s = +30\%$) operation of the DFIG in (a) time domain, and (b) frequency domain.

Figure 3.3 shows the logic diagram of the conventional PUTT scheme, where D_w becomes one if the underreaching element of Relay W detects a fault, and Dp_w becomes one if the overreaching element of Relay W detects a fault, and similarly, D_m becomes one if the underreaching element of Relay M detects a fault. With the frequency deviation of the fault current at large slip values, the conventional PUTT scheme at Relay W will maloperate. Figure 3.4a shows that the impedance trajectory inaccurately enters Zone 1 when there is a balanced fault at 40% of the adjacent line with a fault resistance of 1 Ω when $s = -30\%$. Thus, D_w inaccurately becomes one and causes an instant trip. In summary, Relay W may maloperate based on the conventional PUTT scheme when the DFIG operates at high slip values. However, the distance elements remain reliable when the DFIG operates at small slip values. Figure 3.4b and Figure 3.4c show that the impedance trajectories correctly remain in Zone 2 without entering Zone 1 for balanced Zone 2 faults at 40% of the adjacent line when the DFIG operates at $s = -3\%$ and $s = 0$. As a result, Relay W will operate correctly based on the conventional PUTT scheme for the same external fault when the DFIG operates at small slip values.

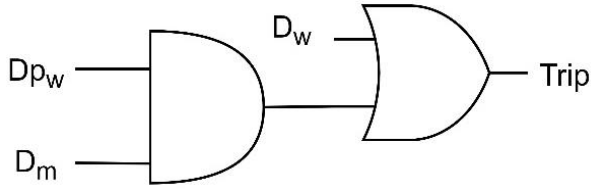

Figure 3.3 Conventional PUTT scheme logic diagram.

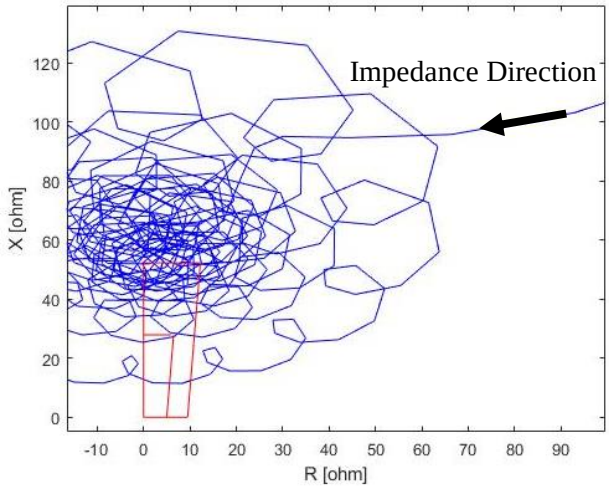
Impedance Direction
X [ohm]
R [ohm]
120
100
80
60
40
20
0
-10
0
10
20
30
40
50
60
70
80
90

(a) $s = -30\%$

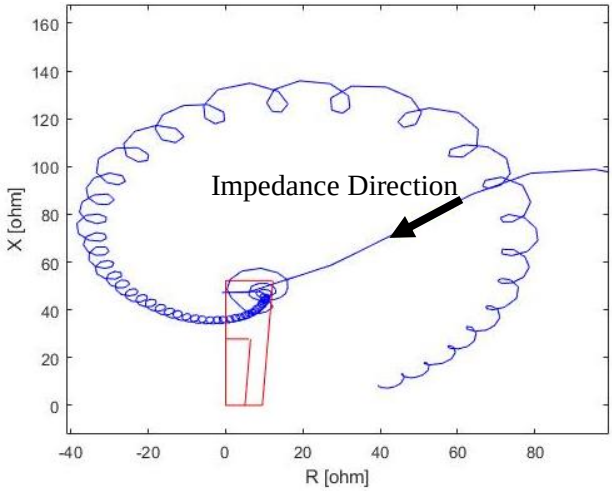
Impedance Direction
X [ohm]
R [ohm]
160
140
120
100
80
60
40
20
0
-40
-20
0
20
40
60
80

(b) $s = -3\%$

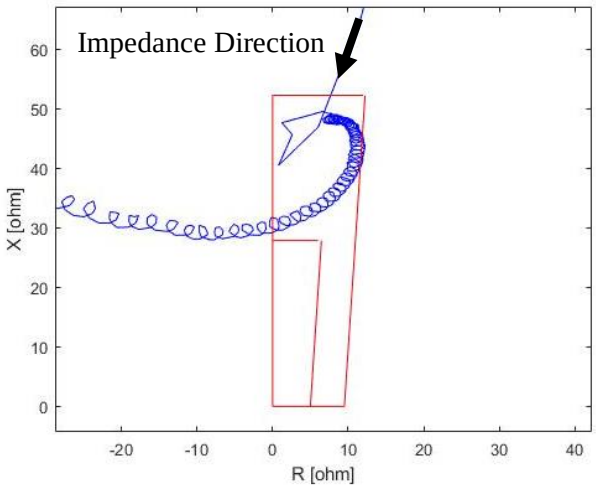

(c) $s = 0$

Figure 3.4 Impedance trajectory calculated by Relay W for a balanced Zone 2 fault at 40% of the adjacent line when (a) $s = -30\%$, (b) $s = -3\%$, and (c) $s = 0$.

3.3.2 Unbalanced Faults

For unbalanced faults, the conventional distance elements remain reliable since the dominant frequency of the fault current remains close to the synchronous frequency under different slip values [19]. Figure 3.5 shows that under an unbalanced ABG fault at 40% of the adjacent line, when the DFIG operates at $s = -30\%$, the impedance trajectory remains in Zone 2 without entering Zone 1. Thus, Relay W will trip correctly under an unbalanced external fault in Zone 2 of the relay even under large slip values.

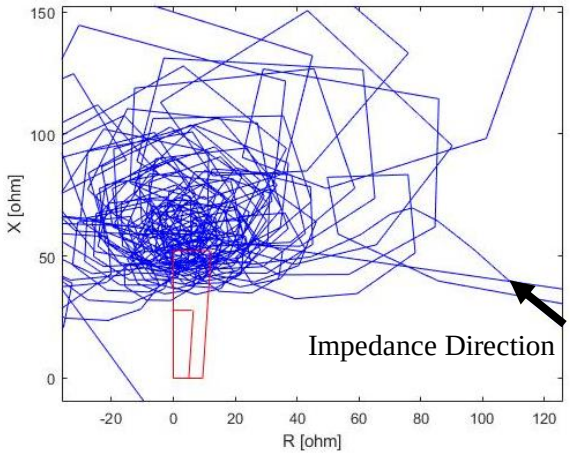

Figure 3.5 Impedance trajectory calculated by Relay W for an unbalanced (ABG) fault at 40% of the adjacent line ($s = -30\%$).

3.4 Modified PUTT Scheme

The presented modified PUTT scheme is based on the conventional PUTT scheme, with the addition of frequency tracking elements f_w and f_m at Relay W and Relay M, respectively, as shown in Figure 3.6.

The frequency tracking elements track the frequency of the currents I_w and I_m measured by Relay W and Relay M, respectively, and if the frequency of I_w (I_m) deviates from a pre-defined range, f_w (f_m) becomes one. This range is defined by an upper and a lower frequency bound corresponding to a slip threshold, s_{th}. When the wind farm operates with small slips, the dominant frequency of the measured fault current is close to the rated frequency. In this case, the conventional PUTT scheme operates correctly. When the DFIG operates at large slip values, the tracked frequencies may significantly deviate from the rated frequency and exceed the pre-defined range. In this case, the frequency tracking element will correctly identify the fault direction and block the maloperation of the distance elements, which are inevitable in a conventional PUTT scheme.

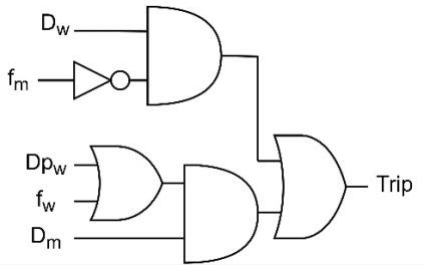

Figure 3.6 The modified PUTT scheme logic diagram.

The operating principle of the developed algorithm is shown in Figure 3.7. In the developed algorithm, local current and voltage measurements at each relay are used to detect faults and distinguish the faults from disturbances such as power swings and load encroachments, using the moving sum approach presented in [54], [36]. After a fault is detected, if $D_w = 1$ and $f_m = 0$, it can be concluded that this is an internal fault and Relay W should trip instantly. Otherwise, in the case that the underreaching element of Relay W maloperates for an external fault in Zone 2 of the relay due to the impedance trajectory incorrectly entering Zone 1, as shown in Figure 3.4a, f_m will become one and correctly block the operation of the underreaching element. D_w becomes zero when the underreaching element of Relay W does not detect a fault in Zone 1. This is the case if (i) an internal fault occurs in the non-overlapping region of the underreaching element of Relay M; (ii) an external fault occurs on the adjacent line; or (iii) a reverse fault occurs. Such cases can be distinguished by identifying whether the fault is in the overlapping region of the underreaching element of Relay M and the overreaching element of Relay

W, similar to the conventional PUTT scheme, or by determining the location of the fault with respect to the Relays M and W using the frequency tracking feature. In the presented PUTT scheme, the frequency tracking element, in addition to the overreaching element, supervises the communication channel. Since D_m corresponds to the underreaching element of Relay M on the grid side, its performance is not affected by the DFIG. In case of an internal fault in the non-overlapping region of the underreaching element of Relay M, Dp_w may become zero due to the maloperation of the overreaching element of Relay W. In such a case, f_w, which corresponds to the frequency tracking element of Relay W, will become one, enabling the trip of the relay. In such a case, if both D_m and f_w become one, it can be concluded that the fault is located in Zone 1 of Relay M and thus it is an internal fault. In case of an external fault on the adjacent line or a reverse fault, similar to the conventional PUTT scheme, D_m will remain zero and therefore, no trip signal will be generated. Under small operating slips, since f_m and f_w become zero, the presented modified PUTT scheme operates similarly to the conventional PUTT scheme.

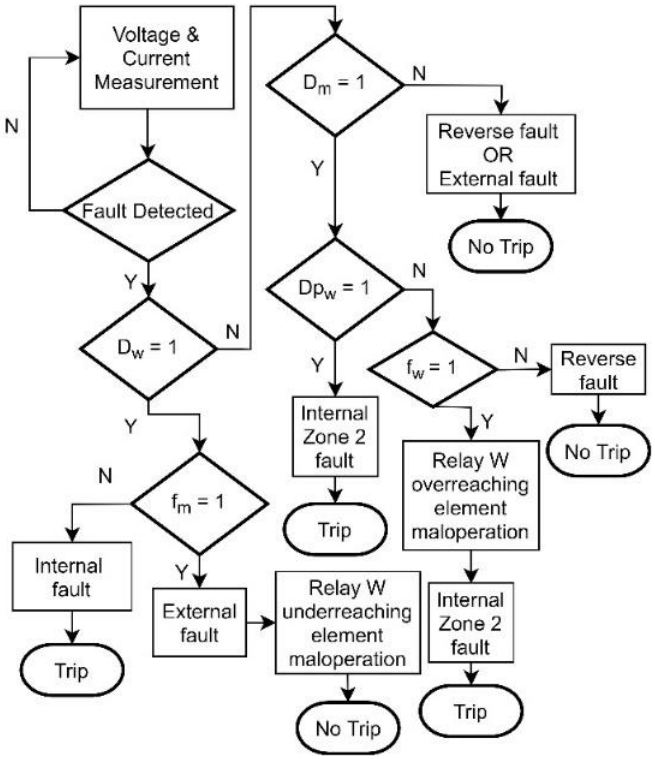

Figure 3.7 The modified PUTT scheme flow chart.

3.5 Simulation Results

In this section, the performance of the developed protection scheme is evaluated under various fault scenarios.

3.5.1 Frequency Tracking Results

To evaluate the performance of the developed relay, a slip threshold $s_{th} = 3\%$ is selected, which corresponds to an upper bound of $62.4\ Hz$ and a lower bound of $57.6\ Hz$ for the operating frequency of DFIG. This setting is selected such that the frequency tracking elements of Relay W and Relay M are not activated for fault scenarios that can be correctly detected by the conventional PUTT scheme. For small negative slip values ($-3\% \leq s \leq 0$), based on (3.3), an external fault at the end of Zone 2 of Relay W when $s = -3\%$ results in the smallest fault current with maximum frequency deviation measured at Relay W. Similarly, for small positive slip values ($0 \leq s \leq +3\%$), based on (3.3), an external fault at the end of Zone 2 of Relay W when $s = 0$ results in the smallest fault current at Relay W. In addition, as shown in Figure 3.4b and Figure 3.4c, the impedance trajectories correctly enter Zone 2 and remain in that zone. Therefore, a conventional PUTT scheme will be able to correctly identify the fault location. For $s < -3\%$ or $s > +3\%$, the frequency tracking elements are correctly activated when a balanced external fault occurs at 40% of the adjacent line. The sudden increase or decrease of the frequency at the instant of the fault is due to the transients introduced by the sudden rise of the fault current, and thus frequency associated with the first cycle after the fault is neglected.

Figure 3.8 shows the instantaneous frequency of the short-circuit current under a reverse fault, an internal fault, and an external fault, with DFIG operating at $s = -30\%$. This slip value corresponds to the maximum frequency deviation in the fault current. For the reverse fault shown in Figure 3.8a, the frequency detected at both relays is close to the rated frequency and the frequency tracking elements remain deactivated for a reverse fault. Figure 3.8b shows that during an internal fault, the frequency tracking element of Relay M remains deactivated, and the one of Relay W becomes activated as the measured frequency, which is $(1 + 30\%) \times 60\ Hz = 78\ Hz$, exceeds the upper bound of the frequency range ($57.6 \leq f \leq 62.4\ Hz$). Similarly, as shown in Figure 3.8c, under an external fault, since frequency at both relays exceeds $62.4\ Hz$, both f_w and f_m become one.

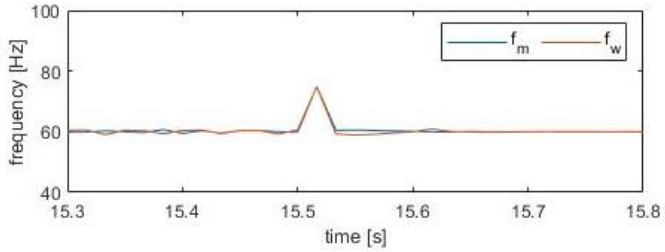

(a) Balanced reverse fault

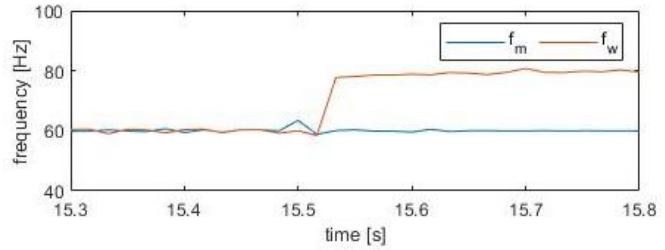

(b) Balanced internal fault

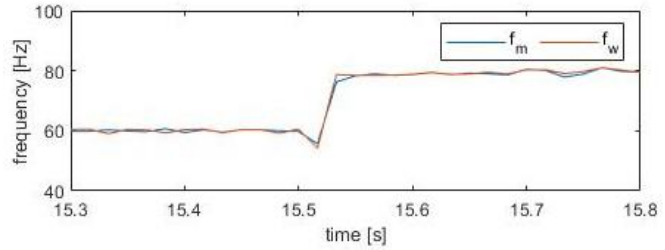

(c) Balanced external fault

Figure 3.8 Frequency of $I_w$and I_m under (a) a balanced reverse fault ($s = -30\%$), (b) a balanced internal fault at 75% of the protected line ($s = -30\%$), and (c) a balanced external fault at 40% of the adjacent line ($s = -30\%$).

3.5.2 Overall Performance

With the reliable performance of the frequency tracking elements, the presented modified PUTT scheme is able to correctly block the malfunctioning of underreaching and overreaching distance elements and prevent inaccurate tripping of the breakers. To prevent the maloperation of the underreaching element of Relay W under balanced external faults in Zone 2 of the relay with DFIG operating at large slip values, as mentioned in section 3.3, the presented scheme blocks the relay operation when the frequency tracking element of Relay M is activated. Furthermore, the presented scheme enables the trip of the relay for internal faults in the non-overlapping region of the underreaching element of Relay M, which are not detected by the conventional PUTT scheme due to

the failure of the overreaching element of Relay W. The developed scheme uses the frequency tracking elements to supervise the communication channel and to generate a trip signal in case of the overreaching element failure. The developed scheme inherits the advantages of the conventional PUTT scheme and requires a low communication bandwidth, as only two binary signals (D_m and f_m) are communicated.

3.6 Conclusions

This chapter presented a modified PUTT scheme to address the protection of the transmission lines connecting DFIG-based wind farms. The developed scheme operates reliably under different operating slips and requires a low communication bandwidth. The study shows that the developed scheme properly addresses the protection issues associated with the distance elements, caused by the frequency deviation of the fault current. By adding the frequency tracking elements to the conventional PUTT scheme, the modified scheme correctly blocks the maloperation of the distance elements during external faults, enables the trip of the relay during internal faults, and significantly improves the security of the relay at the wind farm side.

Chapter 4
Modified Distance Protection Scheme

4.1 Introduction

Non-solid faults in transmission lines are not rare and can cause severe safety hazards [24]. For example, trees touching power lines can cause faults that conventional distance relays are generally insensitive to, and due to the unpredictable nature of RESs and the characteristics of the converters, this protection challenge becomes more complicated in power systems with integrated RESs and may result in failure of conventional distance relays [23][24].

Several adaptive distance relaying schemes are proposed to address the impedance error caused by the fault resistance in AC systems connecting synchronous generators [56][57][58]. The existing schemes, which address the protection of synchronous generators against non-solid faults, do not apply to systems connecting CBRs. The reason is that in these schemes, a synchronous generator is modeled as a voltage source with a fixed impedance, but a CBR is modeled as a current source in parallel with a variable impedance. [59] proposes that the equivalent impedance of the wind farm can be estimated based on the number of connected WTGs and zone boundaries can be adjusted based on the impact of fault resistances. [60] proposes that the fault resistance can be calculated based on the power injection from both sides of the transmission line. While fault resistance can be explicitly calculated, this method requires a communication channel. [61] proposes a communication-less scheme that can accurately estimate the equivalent impedance of various CBRs and then eliminate the impact of the fault resistance on the impedance trajectory based on the phase angle shift of the calculated impedance by conventional distance relays. While this scheme functions accurately with most CBRs, due to the short-circuit characteristics of DFIGs and their fault current frequency deviation, the circuit analysis using phasors calculated by conventional DFT method can be inaccurate.

To determine the accurate phasor of a signal with an off-nominal frequency, [62] proposes a phasor calculation method based on Taylor's series linearization and least-squares technique. [63] proposes that quadratic interpolation in the frequency domain can be used to calculate a correcting coefficient to improve the accuracy of the phasor. [64] proposes an adjustment to the value of the sampled input before applying the DFT method to achieve more accurate phasors. While all the aforementioned phasor estimation methods present accurate results, they require raw instantaneous measurements and significant computation capacity. To eliminate the error in the impedance calculated by conventional

distance relays, which is caused by fault resistances, in a system connecting DFIGs, a less complicated phasor estimation method is desired to achieve a faster operation and a less accurate method is acceptable as long as the overall protection scheme operates reliably.

This chapter presents a reliable protection scheme that addresses the protection challenges associated with distance relays at the terminal of DFIG-based WTGs during non-solid faults. This protection scheme is developed based on the adaptive distance protection scheme proposed by [61] with necessary improvements to correct the phasor estimation inaccuracy caused by the frequency deviation associated with the short-circuit characteristics of DFIG-based WTGs.

4.2 Test System

The test system used in the studies of this chapter is shown in Figure 4.1. A DFIG-based wind farm is connected to the AC grid through two segments of 100 km transmission lines. The distance relay of interest, Relay W, is located at the WTG side of the protected segment of the transmission line. The underreaching element of relay W covers 80% of the protected line (Zone 1), and the overreaching element of relay W covers 140% of the protected line (Zone 2). The parameters of the system are provided in Table 4.1. Type III WTG model from [26] is implemented in this test system with a feasible slip range of $\pm 20\%$ under a wind speed range of $4 - 25\ m/s$. The maximum and minimum slip values are set as $+30\%$ and -30%, respectively $\pm\ 30\%$.

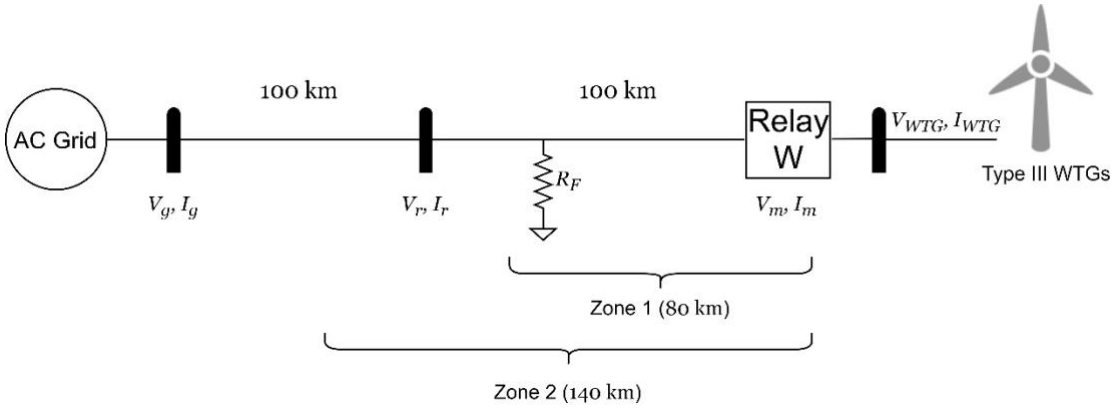

Figure 4.1 Test system transmission lines connecting Type III WTGs.

Table 4.1 Parameters of the test system

Component	Parameter	Value
Type III WTG [26]	Rated power	2 MVA

	Rated voltage	0.69 kV
	Rated wind speed	11 m/s
	Wind speed range	4 – 25 m/s
	Slip range	+/- 20%
Wind Farm	Number of units	100
	Rated power	200 MVA
	Rated voltage	33 kV
AC Grid	Rated voltage	230 kV
	Rated frequency	60 Hz
Transmission Lines	Positive-/negative-sequence impedance	$0.1\angle 87°$ pu / 100 km
	Zero-sequence impedance	$0.37\angle 73°$ pu / 100 km

4.3 Problem Statement

With the existence of a fault resistance, the fault no longer short-circuits the transmission line and there will be a voltage drop across the fault resistance. Thus, the measured voltage at the relay location no longer equals the total voltage drop between the relay and the fault location, and consequently, (3.1) and (3.2) become inaccurate in estimating the positive-sequence impedance between the fault and relay location. This may result in the maloperation of the distance relay.

In this section, the protection challenges associated with the impact of the fault resistance and inaccurate phasor calculation due to the off-nominal frequency of the fault current caused by the short-circuit characteristics of the DFIGs, on the measured impedance by a conventional distance relay, are discussed. Furthermore, the performance of the conventional distance relaying scheme implemented in the wind farm side relay of the test system is evaluated.

4.3.1 Impact of the Fault Resistance on Measured Impedance

When the fault resistance is not zero, the measured impedance by a conventional distance relay will be different from the actual impedance. For the test system shown in Figure 4.1, the relationship between the actual impedance (Z_{actual}) and the measured impedance (Z_m) can be expressed as

$$Z_m = Z_{actual} + R_F \frac{I_r + I_m}{I_m} = Z_{actual} + R_F \frac{I_F}{I_m} = Z_{actual} + \Delta Z, \quad (4.1)$$

where R_F is the fault resistance, I_r is the current from the remote source, I_m is the current supplied from the local source, and I_F is the current through the fault resistance. The phasor diagram depicted in Figure 4.2 illustrates the impact of the fault resistance on a measured impedance by the conventional distance relays. Z_{actual}, Z_m, and ΔZ follows the relationship discussed in (4.1), where Z_{actual} is proportional to the line impedance and has the same phase angle θ_{line} as the line impedance. R_m and X_m are the resistance and reactance of the measured impedance and α is the phase angle of the error term ΔZ. If the impedance error term ΔZ is calculated, the actual impedance during non-solid faults can be determined by post-processing the measured impedance by the conventional distance relay.

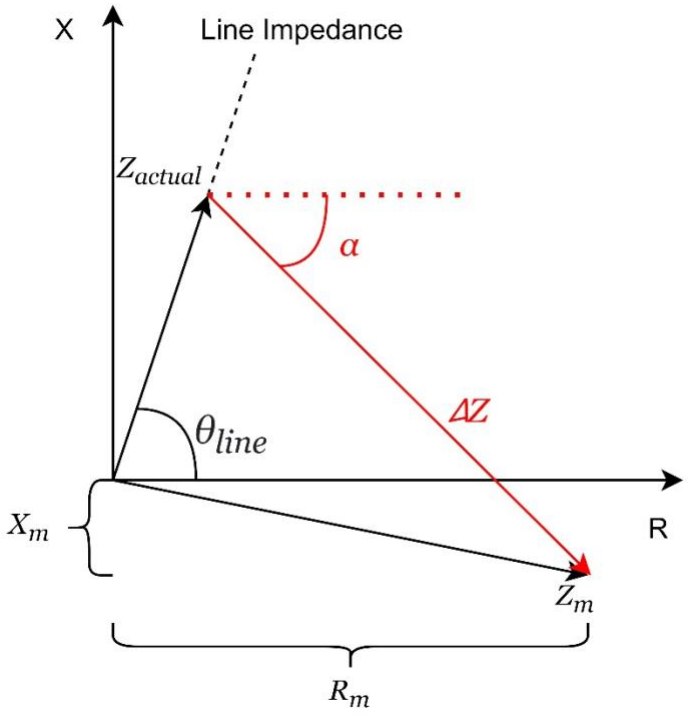

Figure 4.2 The impact of fault resistances on a measured impedance by the conventional distance relays.

Figure 4.3 shows an example of a balanced fault located at the end of Zone 2 of the transmission line connected to the DFIG-based WTG ($s = -20\%$), with a fault resistance of 100 Ω. It can be seen that with the fault resistance, the impedance trajectory measured by the conventional distance relay significantly deviates from the actual impedance, which is proportional to the line impedance. Thus, the impedance trajectory fails to enter the correct zones of the distance relay and consequently the corresponding relay maloperates.

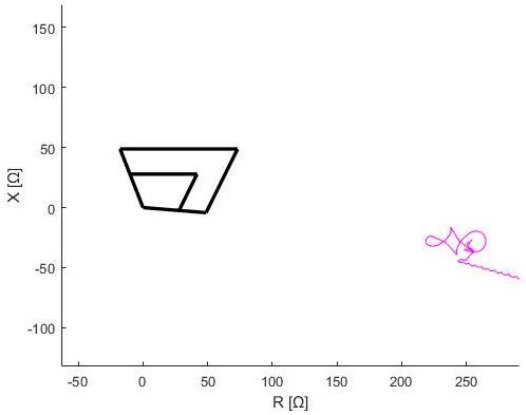

Figure 4.3 Impedance trajectory for a balanced fault located at 140% of the line connected to the WTG with $R_F = 100\ \Omega$ and $s = -20\%$.

4.3.2 Phasor Calculation Error Due to the Off-nominal Frequency of the Current

In addition to the impedance error due to fault resistance, a distance relay utilized for the protection of a transmission line connected to a DFIG-based wind farm must resolve the issue associated with the short-circuit characteristics of DFIGs as discussed in section 3.3. With the frequency deviation during a three-phase fault, the phasors calculated using DFT will be different from their actual values. Since the conventional distance relay and the developed protection scheme in this chapter rely on phasor calculations, significant errors may occur in the measured impedance leading to the maloperation of the relays. Thus, it is important to pre-process the measured current and correct the estimated phasor to eliminate the error in the calculated impedance.

A fault with a small fault resistance will cause a significant deviation in the frequency of the short-circuit current, while a large fault resistance may help to damp the off-nominal frequency. With $s = -20\%$, Figure 4.4 shows that a fault close to the terminal of a DFIG-based wind farm at $t = 5\ s$ with a large fault resistance of $100\ \Omega$ results in a current measurement with the nominal frequency of $60\ Hz$, while Figure 4.5 shows that a remote fault at $t = 5\ s$ with a small fault resistance of $2\ \Omega$ results in a current measurement with an off-nominal frequency. The peaks of the measured frequencies at $t = 5\ s$ in both figures are caused by the sudden increase of the fault current within the first cycle. Therefore, the first cycle after the fault is neglected in the protection scheme presented in this chapter.

It can be concluded that for a fault with a large fault resistance, the protection challenge is mainly associated with the error term ΔZ, as discussed in section 4.3.1, and for a fault with a small fault resistance, the protection challenge is mainly associated with inaccurate phasor estimation caused by

the frequency deviation of the measured current. Thus, for a transmission line connected to a DFIG-based WTG, to ensure reliable performance of the relay that is close to the wind farm for a wide range of fault resistances, a modified distance protection scheme is needed.

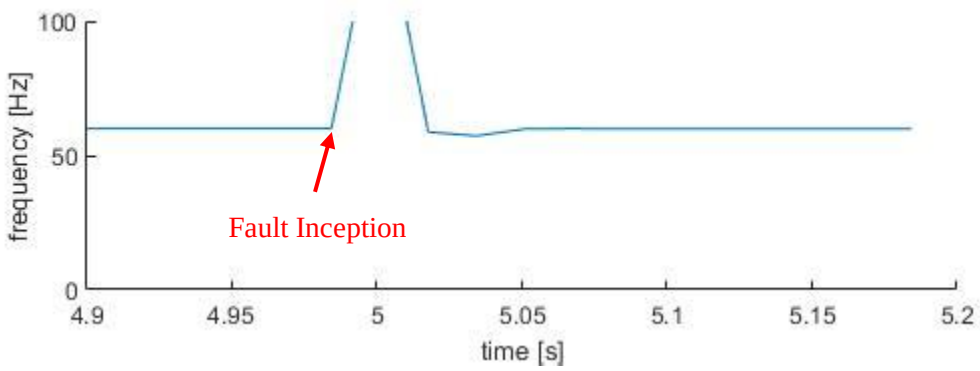

Figure 4.4 Frequency of the measured current for a balanced local fault (4% of the line connected to the WTG) with $R_F = 100\ \Omega$ and $s = -20\%$.

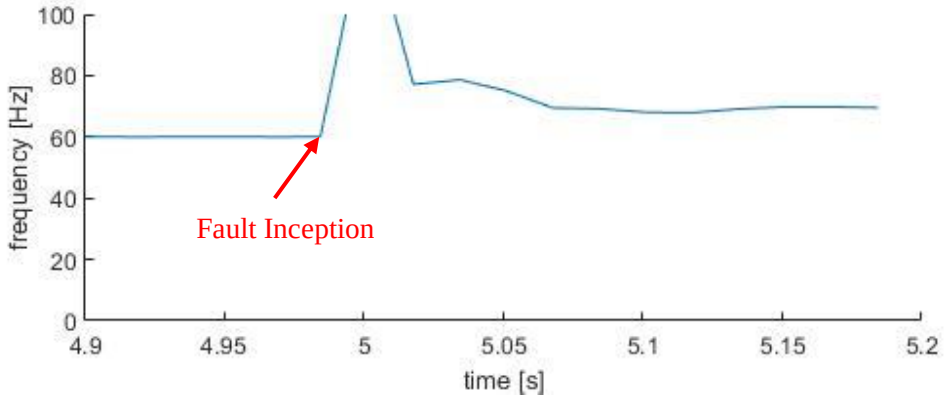

Figure 4.5 Frequency of the measured current for a balanced remote fault (140% of the line connected to the WTG) with $R_F = 2\ \Omega$ and $s = -20\%$.

4.4 Modified Distance Protection Scheme

In this section, a modified distance protection scheme is presented that addresses the challenges discussed in section 4.3. The presented scheme consists of two major components: i) a phasor correction component that solves the protection challenge associated with phasor calculation error due to the off-nominal frequency of the fault current caused by the short-circuit characteristics of the DFIG, and ii) a fault resistance elimination component that eliminates the impact of fault resistance on the measured

impedance by a conventional distance relay. The overall protection scheme provides reliable protection of the transmission line under various fault scenarios, different slip values, and a wide range of fault resistances.

4.4.1 Phasor Correction Component

Assume the given signal $x(t)$ is at a frequency of $\omega = 2\pi f$, which is different from the nominal frequency $\omega_0 = 2\pi f_0$. With a phasor of $X = \frac{X_m}{\sqrt{2}}\angle\varphi$, $x(t)$ can be written as

$$x(t) = X_m \cos(\omega t + \varphi), \tag{4.2}$$

$$\omega = \omega_0 + \Delta\omega\,. \tag{4.3}$$

Using the conventional DFT method, X_r, which is the phasor of $x(t)$ with x_r as the first sample in the sampling window, can be calculated as

$$X_r = \frac{\sqrt{2}}{N}\sum_{k=r}^{r+N-1} x_k e^{-jk\omega_0\Delta t}, \tag{4.4}$$

$$\begin{aligned} x_k = x(k\times\Delta t) = x(t) &= \sqrt{2}Re\left\{\frac{X_m}{\sqrt{2}}e^{j(\omega t+\varphi)}\right\} = \sqrt{2}Re\left\{Xe^{j\omega t}\right\} \\ &= \frac{\sqrt{2}}{2}\left(Xe^{jk\omega\Delta t} + X^* e^{-jk\omega\Delta t}\right), \end{aligned} \tag{4.5}$$

where X is the accurate phasor of $x(t)$, X^* is the complex conjugate of X, and N is the number of samples in the sampling window, and Δt is the interval between two adjacent samples. By substitute (4.5) into (4.4) and rearranging the expression, with the off-nominal frequency ω, the calculated phasor X_r' using the conventional DFT method can be found as [65]

$$X_r' = PXe^{jr(\omega-\omega_0)\Delta t} + QX^* e^{-jr(\omega+\omega_0)\Delta t}\,, \tag{4.6}$$

$$P = \left\{\frac{\sin\frac{N(\omega-\omega_0)\Delta t}{2}}{N\sin\frac{(\omega-\omega_0)\Delta t}{2}}\right\} e^{j(N-1)\frac{(\omega-\omega_0)\Delta t}{2}}, \tag{4.7}$$

$$Q = \left\{\frac{\sin\frac{N(\omega+\omega_0)\Delta t}{2}}{N\sin\frac{(\omega+\omega_0)\Delta t}{2}}\right\} e^{-j(N-1)\frac{(\omega+\omega_0)\Delta t}{2}}. \tag{4.8}$$

The error in the calculated phasor X_r', as compared to the actual phasor X, is mainly due to the second term in (4.6). The factor P in the first term of (4.6) whose detailed expression is shown in (4.7) is around 1 when $\Delta\omega$ is small. Thus, the error in the calculated phasor can be eliminated by a filter that

dynamically averages X_r' over one cycle ($T = \frac{2\pi}{\omega+\omega_0}$) to cancel out the second term in (4.6). The procedure to use the averaging filter to reduce the phasor calculation error, corresponding to the off-nominal frequency of the current is shown in Figure 4.6. The input signal is assumed to be $x(t)$. The instantaneous frequency $f(t)$ can be calculated by tracking the peaks of $x(t)$ at each cycle. Then, phasor X_r' is calculated using the conventional DFT method based on the nominal frequency f_0. With the instantaneously tracked frequency $f(t)$, the frequency of the second term in (4.6) is calculated as $(f(t) + f_0)$. The period of the second term of (4.6), which is represented as $T(t)$, is calculated as $1/(f(t) + f_0)$. By setting the window length of the averaging filter equal to $T(t)$, the second term (error term) of (4.6) is eliminated. Furthermore, even though the factor P in the first term of (4.6) is around 1, the accuracy of the corrected phasor can be improved by dividing the averaged phasor by factor P, which is obtained in (4.7).

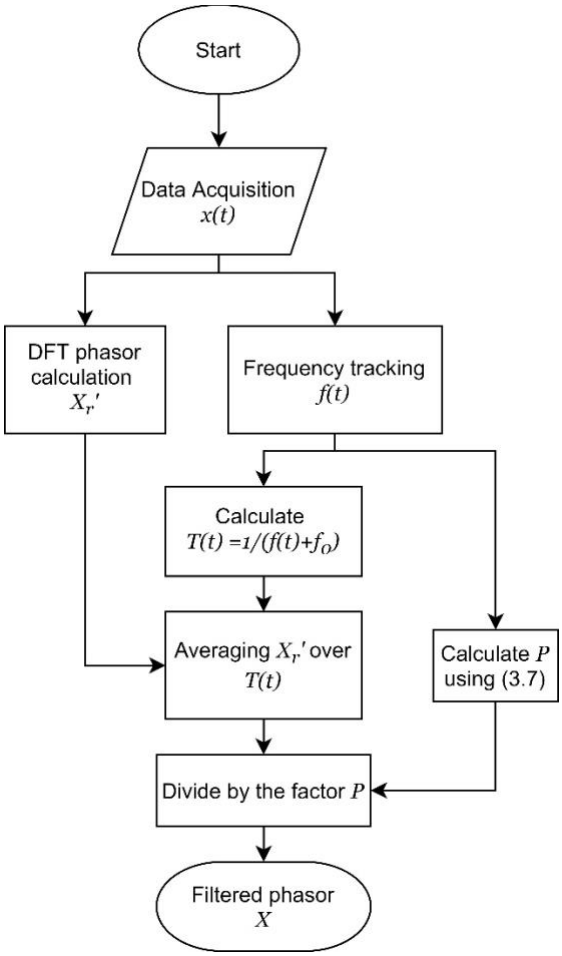

Figure 4.6 Phasor calculation accuracy improvement procedure.

As discussed in section 4.3.2, due to the short-circuit characteristics of the DFIG, the off-nominal frequency occurs in the measured current during a balanced fault when the fault resistance is small. Thus, the aforementioned averaging filter is applied to the current measured at Relay W in the test system shown in Figure 4.1 to correct the current phasor before impedance calculations. Figure 4.7 shows the current phasor magnitude before and after applying the averaging filter. It can be seen that the original phasor calculated using the conventional DFT method has oscillations with a frequency of 132 Hz, which is equal to $(f(t) + f_0)$, as the off-nominal frequency $f(t)$ is around 72 Hz during the fault, and the rated frequency f_0 for the test system is 60 Hz. The oscillations mainly correspond to the second term (error term) in (4.6), and it can be seen that the filtered current phasor has a much smoother waveform without the oscillations.

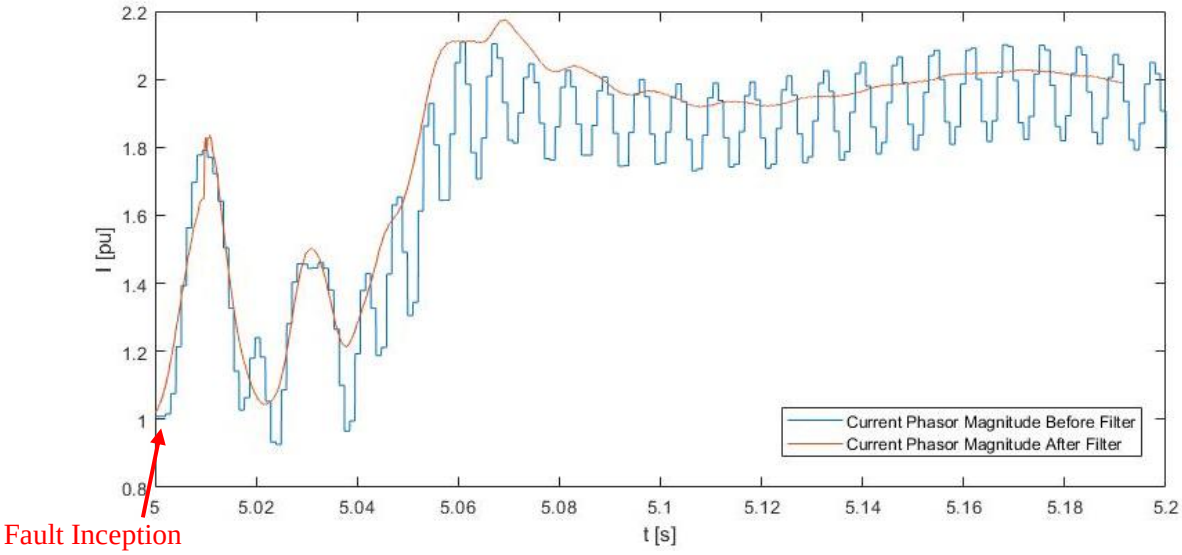

Figure 4.7 Current phasor magnitude before and after filter with a balanced fault located at 140% of the line connected to the WTG with $R_F = 2\,\Omega$ and $s = -20\%$.

4.4.2 Fault Resistance Elimination Component

The fault resistance elimination component used in this modified distance protection scheme is based on the one proposed in [61]. In [61], an adaptive relaying method is proposed to correct the impedance error caused by fault resistances in systems with Type IV WTGs. In [61], the equivalent source impedance of CBRs is estimated using a pure-fault network model. Similar to [61], in the modified distance protection scheme of this thesis, a pure-fault network model will be used to determine the equivalent source impedance of the DFIG connected to the test system shown in Figure 4.1, and the

actual distance between the fault and relay location is determined after eliminating the impact of the fault resistance.

Using the phasor diagram shown in Figure 4.2, the magnitude of the actual impedance is

$$|Z_{actual}| = \frac{X_m - R_m \times \tan\alpha}{\sin\theta_{line} - \cos\theta_{line} \times \tan\alpha}, \tag{4.9}$$

where the only unknown variable is α. The phase angle of the actual impedance is similar to the phase angle of the transmission line. Since α is the phase angle of ΔZ and R_F is pure-resistive, α can be calculated as

$$\alpha = angle\left(\frac{I_F}{I_m}\right). \tag{4.10}$$

Therefore, α is determined based on the phase angle difference between the current measured at the local relay and the current flowing through the fault resistance. Thus, to calculate α and consequently to determine Z_{actual}, an accurate estimation of the current flowing through the fault resistance (I_F) is necessary.

Figure 4.8 and Figure 4.9 show the equivalent pre-fault and during-fault circuits of the test system of Figure 4.1. E_{grid} and E_{WTG} represent the grid voltage and voltage generated by the WTG, respectively. $Z_{WTG,pre}$ and $Z_{WTG,f}$ represents the impedance of the DFIG and adjacent transformers before and during a balanced fault, Z_{total} is the total impedance of the transmission lines between the AC grid and the WTG, Z_{grid} is the equivalent impedance of the AC grid. $I_{pre-fault}$ and $V_{pre-fault}$ are the current and voltage measured at the relay location before the fault, I_m and V_m are the current and voltage measured at the relay location during the fault.

Figure 4.10 shows the corresponding pure-fault circuit of the test system of Figure 4.1. $Z_{WTG,pf}$ represents the pure-fault impedance of the DFIG and adjacent transformers, E_F is the voltage at the fault location before the fault [61]. The pure-fault current ΔI (voltage ΔV) is defined as the difference between the pre-fault current (voltage) and the during-fault current (voltage) measured by the relay, that is

$$\Delta I = I_m - I_{pre-fault}, \tag{4.11}$$

$$\Delta V = V_m - V_{pre-fault}. \tag{4.12}$$

ΔI_g is defined in a similar way as the difference between the pre-fault current ($-I_{pre-fault}$) and the during-fault current (I_g) on the grid side, which is only used for derivation purposes and is not required in the developed protection scheme.

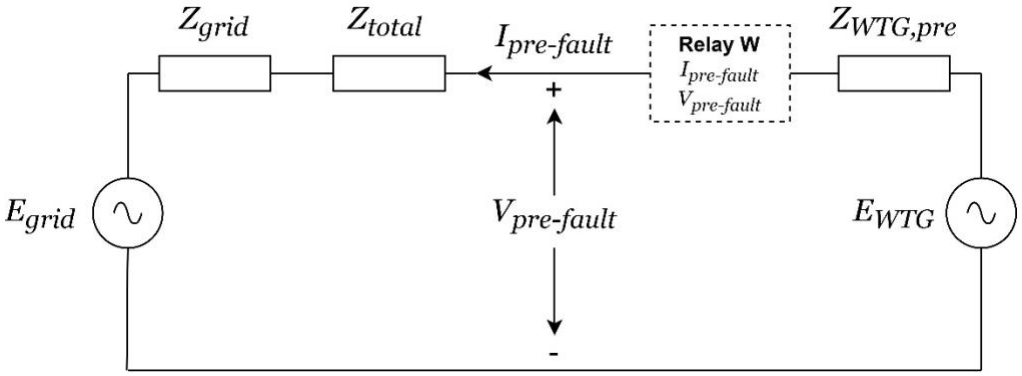

Figure 4.8 The equivalent pre-fault circuit for a balanced fault.

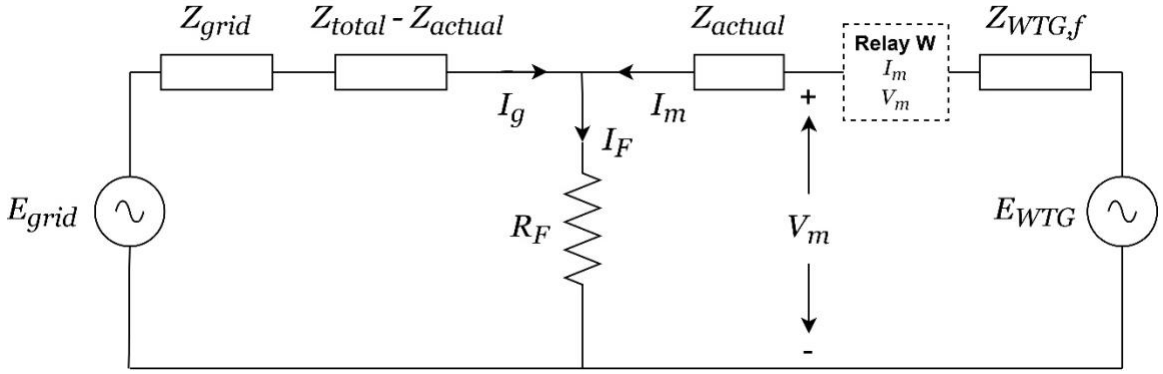

Figure 4.9 The equivalent during-fault circuit for a balanced fault.

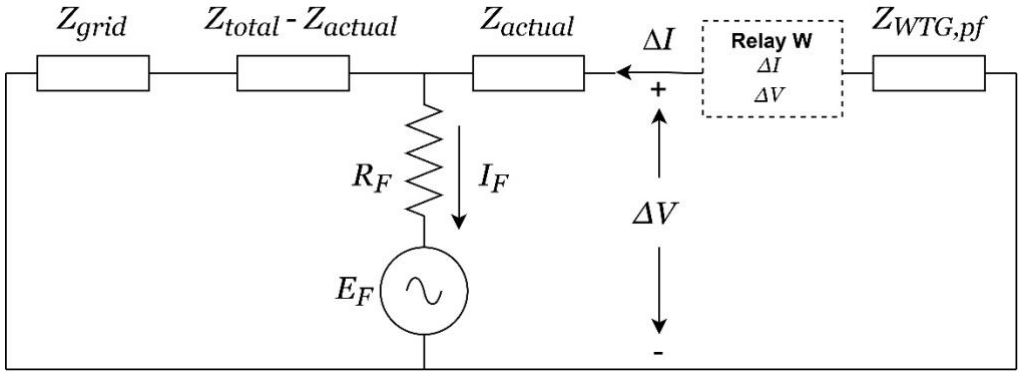

Figure 4.10 The pure-fault circuit for a balanced fault.

Based on the circuits shown in Figure 4.8-Figure 4.10, I_F can be represented as

$$I_F = I_m + I_g = I_m - I_{pre-fault} + I_g - \left(-I_{pre-fault}\right) = \Delta I + \Delta I_g \,. \tag{4.13}$$

By applying the current division rule to the circuit shown in Figure 4.10, ΔI can be represented as

$$\Delta I = I_F \times \frac{Z_{grid} + Z_{total} - Z_{actual}}{Z_{grid} + Z_{total} + Z_{WTG,pf}} = I_m - I_{pre-fault} \,. \tag{4.14}$$

Thus, by substituting (4.11) and (4.13) into (4.14) and rearranging the equation

$$\begin{aligned} Z_{WTG,pf} &= (I_m + I_g) \times \frac{Z_{grid} + Z_{total} - Z_{actual}}{I_m - I_{pre-fault}} - (Z_{grid} + Z_{total}) \\ &= \frac{I_{pre-fault} \cdot (Z_{grid} + Z_{total}) - I_m \cdot Z_{actual} + I_g \cdot (Z_{grid} + Z_{total} - Z_{actual})}{I_m - I_{pre-fault}} \,. \end{aligned} \tag{4.15}$$

From the pre-fault circuit shown in Figure 4.8, the following equation holds:

$$V_{pre-fault} = E_{grid} + I_{pre-fault} \times (Z_{grid} + Z_{total}) \,. \tag{4.16}$$

From the during-fault circuit shown in Figure 4.9, the following equation holds:

$$V_m = E_{grid} - I_g \cdot (Z_{grid} + Z_{total} - Z_{actual}) + I_m \times Z_{actual} \,. \tag{4.17}$$

By substituting (4.16) and (4.17) into (4.15), the pure-fault impedance of the WTG can be calculated as

$$Z_{WTG,pf} = \frac{V_{pre-fault} - V_m}{I_m - I_{pre-fault}} = -\frac{\Delta V}{\Delta I} \,. \tag{4.18}$$

Since ΔV and ΔI are available at Relay W, the pure-fault impedance of the WTG can be calculated locally without any communications.

From (4.14), I_F can be calculated as

$$I_F = \Delta I \times \frac{Z_{grid} + Z_{total} + Z_{WTG,pf}}{Z_{grid} + Z_{total} - Z_{actual}} \,. \tag{4.19}$$

For a strong grid, Z_{grid} is small enough to be neglected in (4.19). The actual impedance between the relay and fault location is a fraction of the total impedance of the protected transmission line. Thus, the phase angle of $Z_{total} - Z_{actual}$ is the same as Z_{total}. Therefore, the phase angle of I_F can be determined as

$$angle(I_F) = angle\left(\Delta I \times \frac{Z_{total} + Z_{WTG,pf}}{Z_{total}}\right) = angle\left(\Delta I \times \left(1 + \frac{Z_{WTG,pf}}{Z_{total}}\right)\right). \quad (4.20)$$

Figure 4.11 - Figure 4.14 show the pure-fault sequence networks for a balanced fault (ABCG), a single-phase-to-ground fault (AG), a phase-to-phase (BC) fault, and a phase-to-phase-to-ground (BCG) fault. The additional subscripts "1", "2", "0", and "a" denote the positive-sequence, negative-sequence, zero-sequence, and phase A components, respectively. The positive-, negative-, and zero-sequence pure-fault impedance of the WTG, $Z_{WTG,pf,1}$, $Z_{WTG,pf,2}$, $Z_{WTG,pf,0}$ are calculated using (4.18) with positive-, negative-, zero-sequence components of ΔV and ΔI.

The pure-fault sequence network for an ABCG fault is shown in Figure 4.11. For a balanced fault, (4.1) is written as

$$Z_{m,1} = \frac{V_{m,1}}{I_{m,1}} = Z_{actual} + R_F \frac{I_{F,1}}{I_{m,1}} = Z_{actual} + \Delta Z\,, \quad (4.21)$$

Thus, for a balanced fault, α, which is the phase angle of ΔZ, can be represented as

$$\alpha = angle\left(\frac{I_{F,1}}{I_{m,1}}\right) = angle\left(\frac{\Delta I_1 * \left(1 + \frac{Z_{WTG,pf,1}}{Z_{total,1}}\right)}{I_{m,1}}\right). \quad (4.22)$$

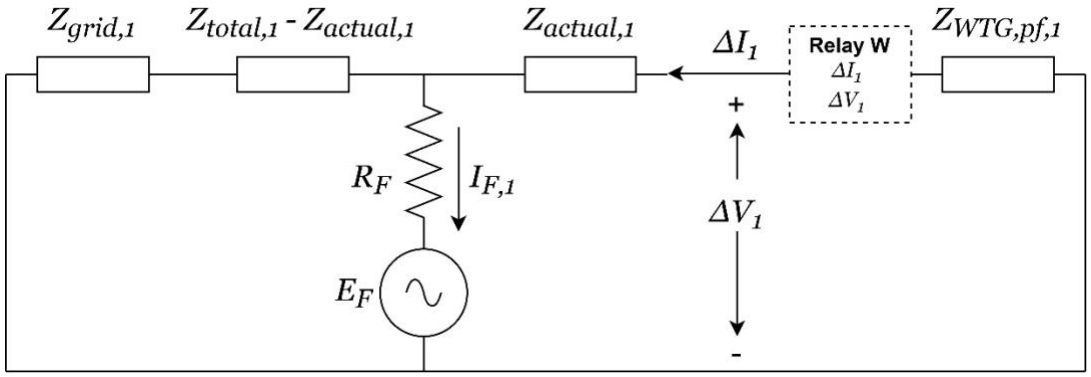

Figure 4.11 Pure-fault sequence network for a balanced (ABCG) fault.

The pure-fault sequence network for an AG fault is shown in Figure 4.12. For an AG fault, (4.1) is written as

$$Z_{m,1} = \frac{V_{m,a}}{I_{m,a} + I_{m,0}K_0} = Z_{actual} + R_F \frac{I_{F,1}}{I_{m,a} + I_{m,0}K_0}\,, \quad (4.23)$$

where K_0 is the zero-sequence current compensation factor and can be calculated as $\frac{Z_{total,0}}{Z_{total,1}} - 1$. Thus, for an AG fault, α can be represented as

$$\alpha = angle\left(\frac{I_{F,1}}{I_{m,a} + I_{m,0}K_0}\right) = angle\left(\frac{\Delta I_1 * \left(1 + \frac{Z_{WTG,pf,1}}{Z_{total,1}}\right)}{I_{m,a} + I_{m,0}K_0}\right). \quad (4.24)$$

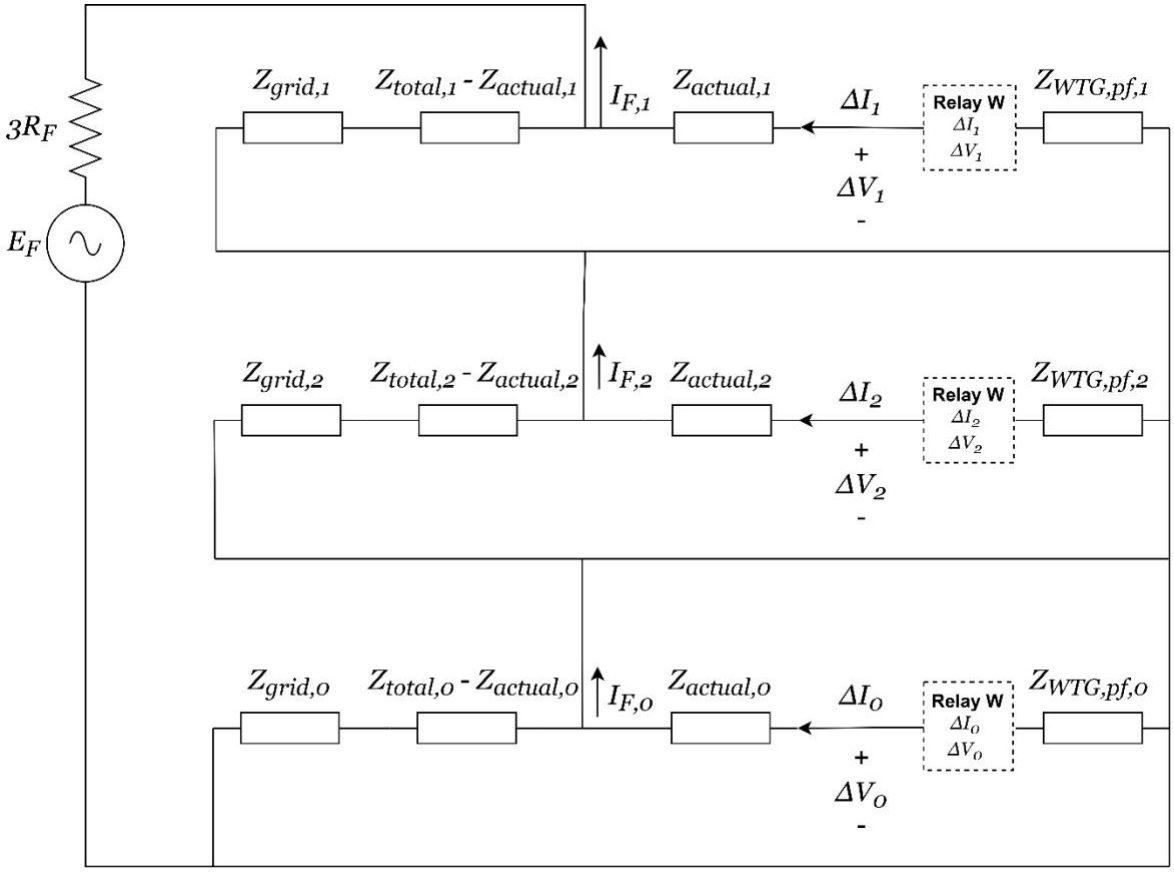

Figure 4.12 Pure-fault sequence network for a single-phase-to-ground (AG) fault.

The pure-fault sequence networks for a BC and a BCG fault are shown in Figure 4.13 and Figure 4.14, respectively. For a BC or BCG fault, (4.1) can be written as

$$Z_{m,1} = \frac{V_{m,1} - V_{m,2}}{I_{m,1} - I_{m,2}} = Z_{actual} + R_F\frac{I_{F,1} - I_{F,2}}{I_{m,1} - I_{m,2}}. \quad (4.25)$$

Since for a BC fault $I_{F,1} = -I_{F,2}$, α can be represented as

$$\alpha = angle\left(\frac{I_{F,1}}{I_{m,1} - I_{m,2}}\right) = angle\left(\frac{\Delta I_1 * \left(1 + \frac{Z_{WTG,pf,1}}{Z_{total,1}}\right)}{I_{m,1} - I_{m,2}}\right). \quad (4.26)$$

For a BCG fault, $I_{F,2}$ can be calculated similarly, using the current division rule in the negative-sequence circuit, as

$$I_{F,2} = \Delta I_2 \times \frac{Z_{grid,2} + Z_{total,2} + Z_{WTG,pf,2}}{Z_{grid,2} + Z_{total,2} - Z_{actual,2}} \ . \quad (4.27)$$

Thus, for a BCG fault, α can be represented as

$$\alpha = angle\left(\frac{I_{F,1} - I_{F,2}}{I_{m,1} - I_{m,2}}\right)$$
$$= angle\left(\frac{\Delta I_1 \times \left(1 + \frac{Z_{WTG,pf,1}}{Z_{total,1}}\right) - \Delta I_2 \times \left(1 + \frac{Z_{WTG,pf,2}}{Z_{total,2}}\right)}{I_{m,1} - I_{m,2}}\right). \quad (4.28)$$

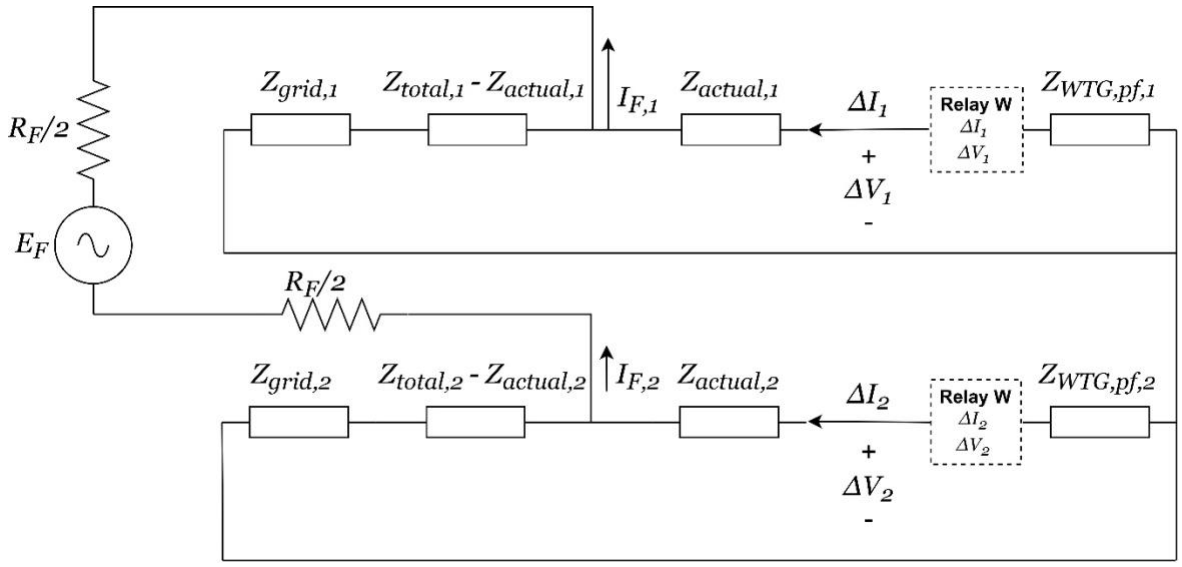

Figure 4.13 Pure-fault sequence network for a phase-to-phase (BC) fault.

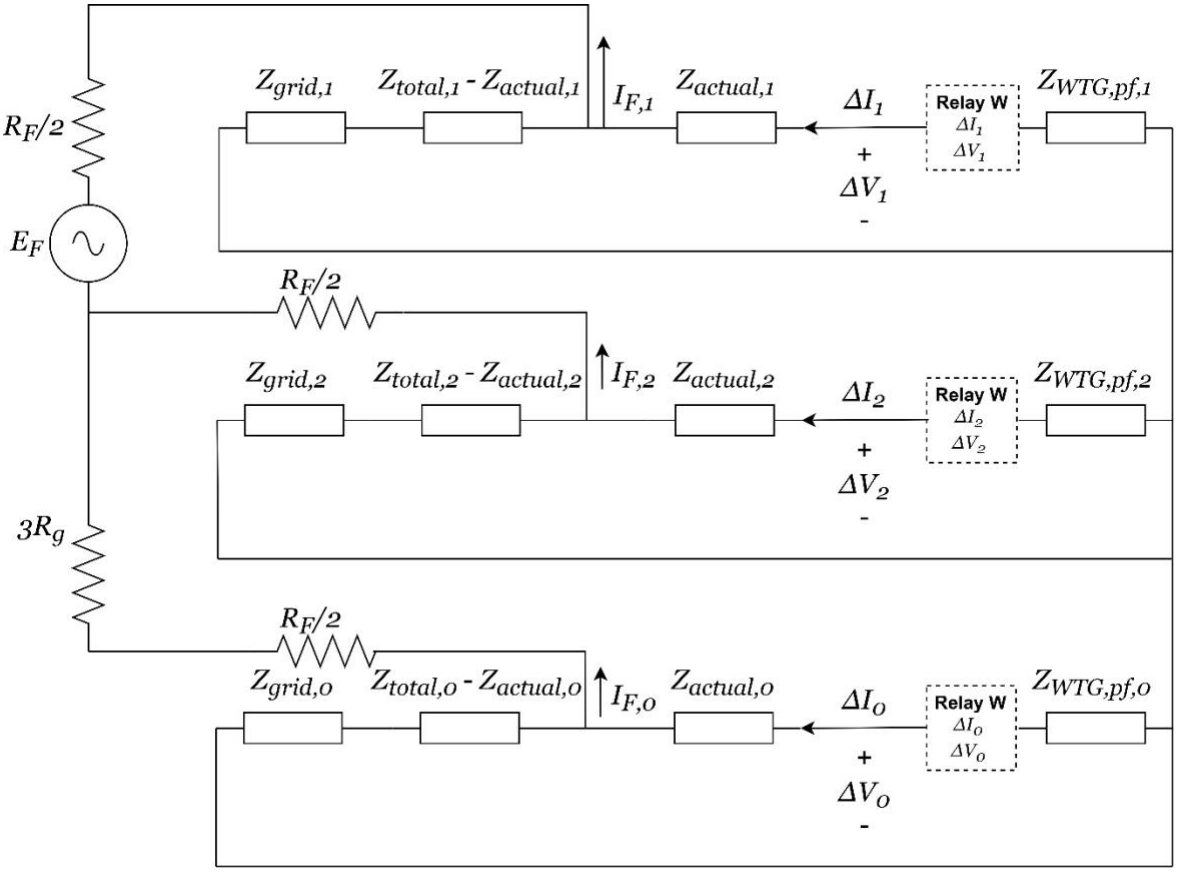

Figure 4.14 Pure-fault sequence network for a phase-to-phase-to-ground (BCG) fault.

The calculation of α for various fault types is summarized in Table 4.2.

Table 4.2 Calculation of α

Fault Type	α
ABCG	$\alpha = angle\left(\frac{\Delta I_1 * \left(1 + \frac{Z_{WTG,pf,1}}{Z_{total,1}}\right)}{I_{m,1}}\right)$
BCG	$\alpha = angle\left(\frac{\Delta I_1 * \left(1 + \frac{Z_{WTG,pf,1}}{Z_{total,1}}\right) - \Delta I_2 * \left(1 + \frac{Z_{WTG,pf,2}}{Z_{total,2}}\right)}{I_{m,1} - I_{m,2}}\right)$
BC	$\alpha = angle\left(\frac{\Delta I_1 * \left(1 + \frac{Z_{WTG,pf,1}}{Z_{total,1}}\right)}{I_{m,1} - I_{m,2}}\right)$

AG	$\alpha = angle\ (\frac{\Delta I_1 * (1 + \frac{Z_{WTG,pf,1}}{Z_{total,1}})}{I_{m,a} + K_0 * I_{m,0}})$

In summary, the following steps shown in Figure 4.15 should be completed to eliminate the impact of the fault resistance on the calculated impedance between the relay and fault location: 1. The fault is detected and the fault type is identified based on the phase angle difference and voltage magnitude difference among the negative-, positive-, and zero-sequence voltages, as proposed in [66]. 2. The conventional distance relay measures the impedance trajectory as Z_m using the current and voltage measurements. 3. The pure-fault impedance of the WTG is calculated using (4.18). 4. Based on the fault type, α is calculated using the corresponding formula in Table 4.2. 5. The actual impedance Z_{actual} is calculated using (4.9).

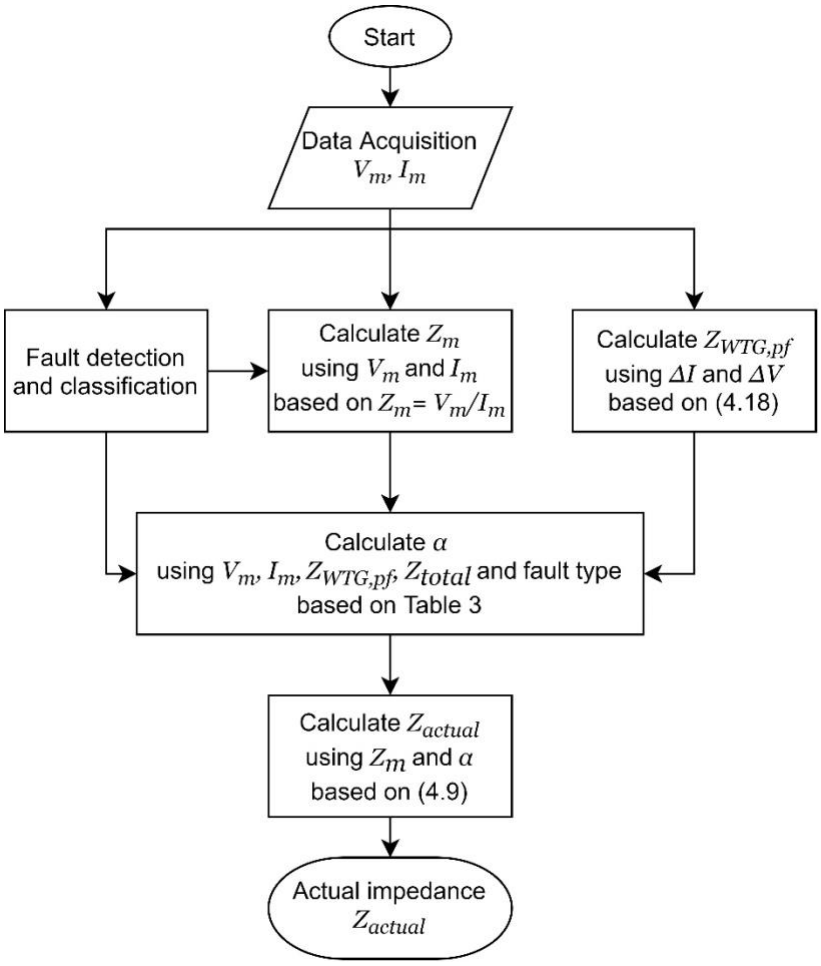

Figure 4.15 Fault resistance impact elimination procedure.

4.4.3 Modified Distance Protection Scheme

The various components of the modified distance protection scheme, which solves the protection problem associated with the error caused by a fault resistance in a transmission line connecting a DFIG, are depicted in Figure 4.16. A fault is detected and the fault type is identified based on the phase angle differences and voltage magnitude differences among the negative-, positive-, and zero-sequence voltages, as proposed in [66]. In [66], the magnitude of negative- and zero-sequence voltages and their differences can be used to identify balanced faults and distinguish between BC and BCG faults; the phase angle difference between negative- and zero-sequence voltages can be used to identify AG or BCG faults; and the phase angle difference between negative- and positive-sequence voltages can be used to further distinguish between AG and BCG faults. Meanwhile, instantaneous voltage $v(t)$ and current $i(t)$ are continuously measured, and instantaneous frequency $f(t)$ of the current is tracked. Voltage and current phasors, V_m and I_m, are calculated using the conventional DFT method. Upper and lower frequency thresholds, f_{max} and f_{min}, are selected to determine if there is a deviation in the frequency from the nominal value. Based on section 3.3.1, f_{max} is selected as $(1 + 3\%)f_0$ and f_{min} is selected as $(1 - 3\%)f_0$, since for small slip values between $\pm 3\%$, a fault with a small fault resistance can be correctly detected by conventional distance relays. If $f(t)$ remains within the thresholds, it may be due to i) a balanced fault with a small slip value, ii) an unbalanced fault, or iii) a balanced fault with a large slip value and a large fault resistance that damps the off-nominal frequency component. Thus, in all of these three scenarios, a conventional relay is used to calculate the impedance Z_m. If Z_m enters a protection zone, a proper trip signal will be generated by a conventional distance relay. If Z_m remains outside the protection zones, this may be due to i) an external fault (reverse fault or outside Zone 2), or ii) an internal fault with a large fault resistance. Thus, the impact of the fault resistance on the measured impedance Z_m is eliminated, as described in section 4.4.2, and the actual impedance Z_{actual} is calculated. If Z_{actual} enters a protection zone, a trip signal will be generated. Otherwise, an external fault will be identified. If $f(t)$ exceeds the upper or lower frequency thresholds caused by a large slip value and a balanced fault, the averaging filter presented in section 4.4.1 is applied to correct the current phasor calculated using the DFT method. Using the corrected current phasor I'_m, corrected impedance Z'_m is calculated. If Z'_m enters a protection zone, a trip signal will be generated. If Z'_m remains outside the protection zone, this may be due to i) an external fault, or ii) an internal fault with a fault resistance that impacts the impedance trajectory but is not large enough to damp the off-nominal frequency component. To correctly identify the fault in the latter scenario, the impact of the fault resistance on Z'_m is eliminated, as described in section 4.4.2, and the actual impedance Z'_{actual} is calculated. If

Z'_{actual} enters a protection zone, a trip signal will be generated. Otherwise, it is an external fault. The presented scheme applies to both Zone 1 and 2 faults. If the protection zone that picks up is Zone 1, an instant trip signal is generated. If the protection zone that picks up is Zone 2, a delayed trip signal is generated to provide backup protection.

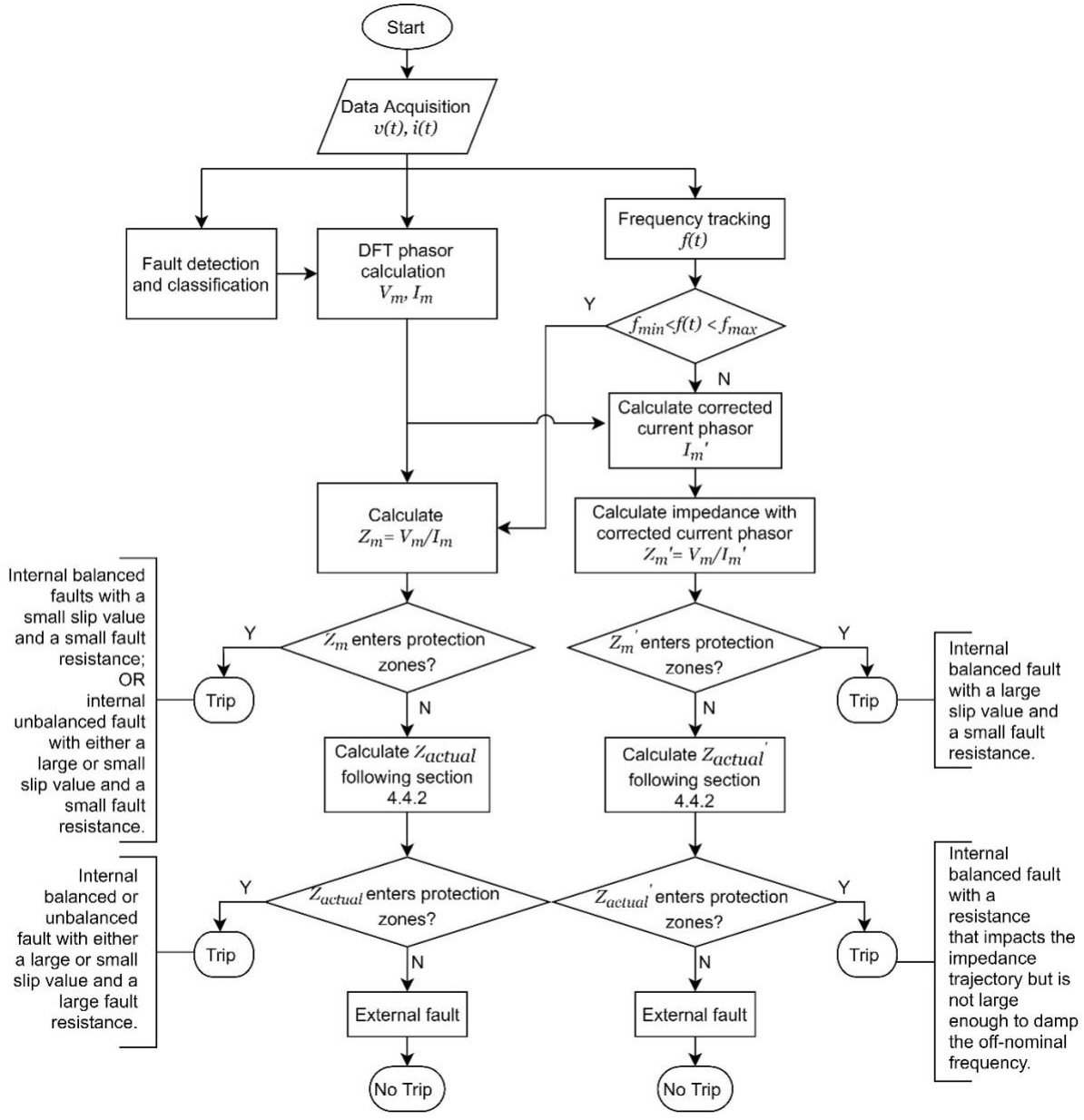

Figure 4.16 Overall workflow for the modified distance protection scheme.

4.5 Simulation Results

This section presents the simulation results of the modified distance protection scheme for four fault scenarios with balanced faults with large, small, and medium resistances, and unbalanced faults with large resistances, respectively, when the DFIG operates at a large slip value. The test system is as shown in Figure 4.1.

4.5.1 Balanced Faults with Large Resistance

Two fault scenarios are selected to evaluate the performance of the modified distance element. The fault scenarios are the ones that result in the largest impedance error. Based on (3.1), a large impedance errors ΔZ is caused by a large R_F and a small I_m. For a DFIG with a slip range of $-20\% \leq s \leq +20\%$, based on (3.3), for negative slip values, I_m is the smallest when $s = -20\%$, and for positive slip values, I_m is the smallest when $s = 0$. When $s = 0$, DFIG can be seen as a SCIG with no frequency deviation, and the fault resistance elimination component functions properly. Also, according to ohm's law, I_m is small when Z_{actual} is large, and Z_{actual} depends on the distance between the fault and the relay location. Thus, for the test system shown in Figure 4.1, for a Zone 2 fault, the largest ΔZ occurs when $s = -20\%$ for a fault located at 140% of the line, which is the furthest reach of the relay. For a Zone 1 fault, the largest ΔZ occurs when $s = -20\%$ for a fault located at 80% of the line, which is the furthest reach of Zone 1.

As mentioned in section 4.3.1, when the fault resistance is large, significant error ΔZ occurs in the calculation of the impedance by conventional distance relays. With the modified distance protection scheme shown in Figure 4.16, for a fault with a large fault resistance, Z_{actual} is calculated based on Z_m using the original phasors without the averaging filter, since the off-nominal frequency in the current measurement is damped by the large fault resistance as discussed in section 4.3.2.

Figure 4.17 shows the impedance trajectory of a conventional distance relay and the modified distance protection scheme for an ABCG fault located at 140% of the line with $R_F = 100\ \Omega$ and $s = -20\%$. Figure 4.18 shows the impedance trajectory of a conventional distance relay and the modified distance protection scheme for an ABCG fault located at 80% of the line with $R_F = 100\ \Omega$ and $s = -20\%$. With a large fault resistance, as mentioned in section 4.4.3, there is no frequency deviation in the fault current, and the impedance trajectory Z_{actual} calculated using the modified distance protection scheme correctly falls at the edge of Zone 2 (140% of the line) and Zone 1 (80% of the line) and remains in the zones for the duration of the faults.

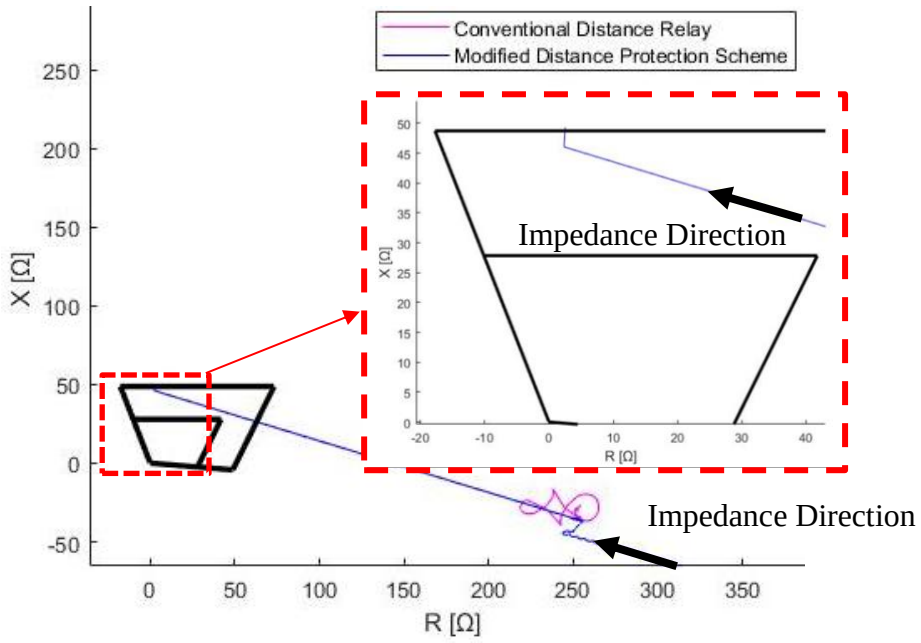

Figure 4.17 Impedance trajectory of a conventional distance relay and the modified distance protection scheme for an ABCG fault located at 140% of the line with $R_F = 100\ \Omega$ and $s = -20\%$.

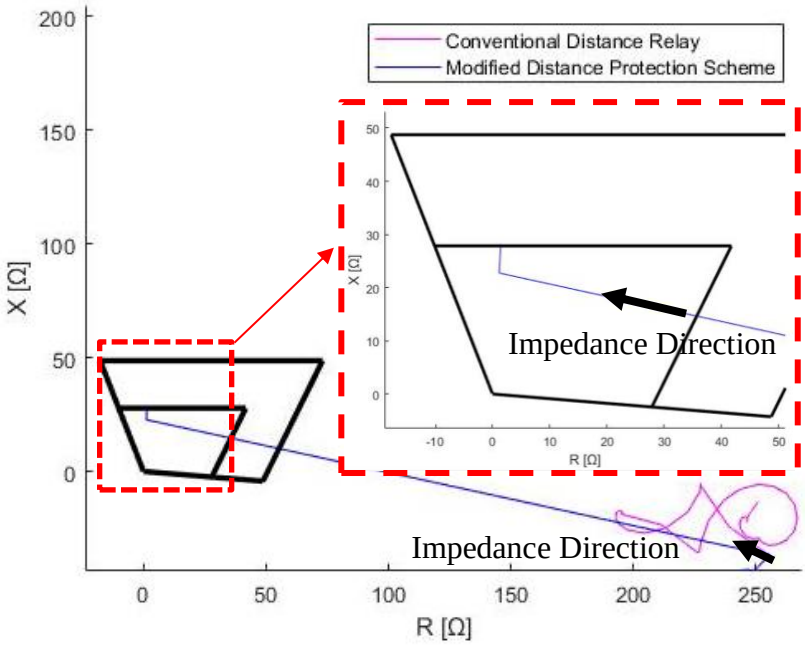

Figure 4.18 Impedance trajectory of a conventional distance relay and the modified distance protection scheme for an ABCG fault located at 80% of the line with $R_F = 100\ \Omega$ and $s = -20\%$.

4.5.2 Balanced Faults with Small Resistance

As mentioned in section 4.3.2, when the fault resistance is small, a frequency deviation will occur in the fault current due to the DFIG's short-circuit characteristics, and the problem of phasor calculation error can be solved using the averaging filter presented in section 4.4.1. However, when the fault resistance is significantly small, the measured impedance Z_m might be in phase with the line impedance, in which case α equals θ_{line}. If α equals θ_{line}, Z_{actual} can no longer be calculated using (4.2) since the denominator goes to zero. Thus, as shown in Figure 4.16, when the fault resistance is significantly small, the impact of the fault resistance on the calculated impedance can be neglected. In such a fault scenario, the impedance trajectory calculated using the filtered phasor Z'_m will correctly enter the protection zone.

The impedance trajectory obtained from the corrected phasors and the original impedance trajectory calculated by the conventional distance relay without the averaging filter are shown in Figure 4.19. It can be observed that without the averaging filter, the original impedance trajectory incorrectly enters Zone 1 for a Zone 2 fault. With the averaging filter, the corrected impedance trajectory does not enter Zone 1 and remains within Zone 2 of the relay.

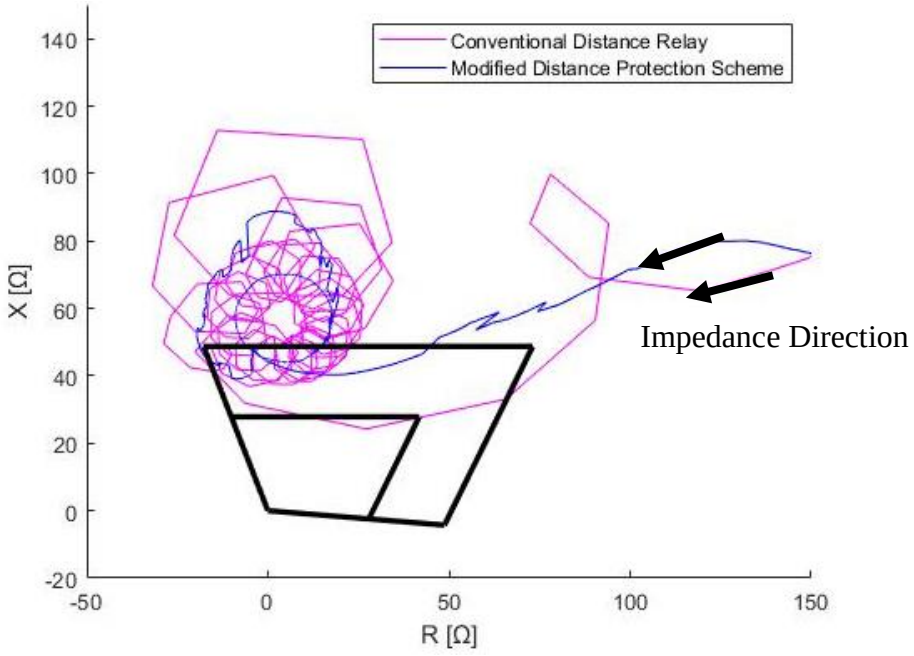

Figure 4.19 Impedance trajectory of a conventional distance relay and the modified distance protection scheme for an ABCG fault located at 140% of the line with $R_F = 2\ \Omega$ and $s = -20\%$.

4.5.3 Balanced Faults with Medium Resistance

In this fault scenario, the fault resistance is neither large enough to fully damp the off-nominal frequency in the fault current nor small enough to not impact the measured impedance. Therefore, for such fault scenarios, Z'_{actual} is calculated based on Z'_m with the corrected phasors. In Figure 4.20, with a fault resistance of 8 Ω, the impedance trajectory of a conventional distance relay fails to enter Zone 2 for an ABCG fault located at 140% of the line, while the impedance trajectory of the modified distance protection scheme correctly enters Zone 2. Due to the sudden change in the fault current and measured voltage when the fault occurs, the first cycle after the fault is neglected. In Figure 4.21, with a fault resistance of 8 Ω, the impedance trajectory of a conventional distance relay fails to enter Zone 1 for an ABCG fault located at 80% of the line, while the impedance trajectory of the modified distance protection scheme correctly enters Zone 1.

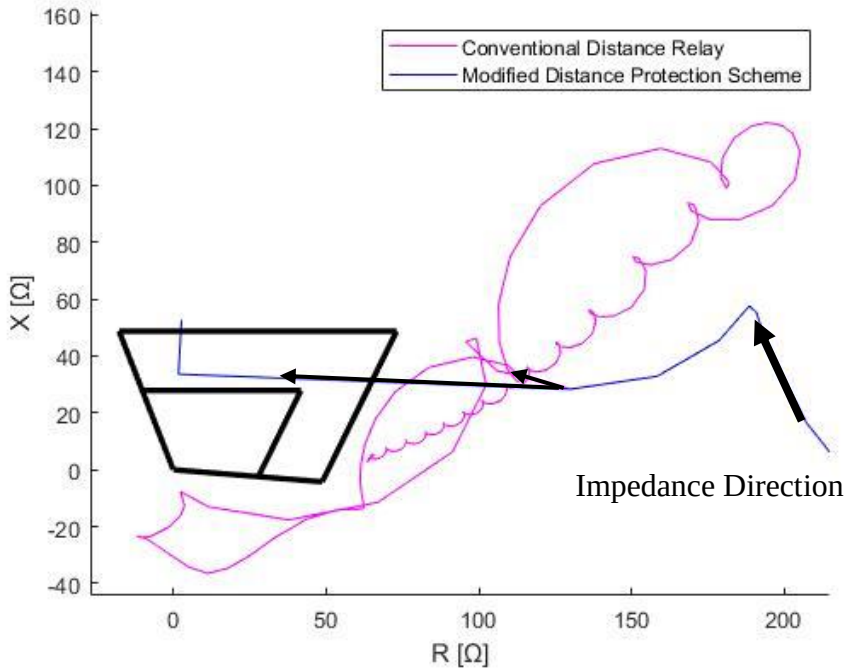

Figure 4.20 Impedance trajectory of a conventional distance relay and the modified distance protection scheme for an ABCG fault located at 140% of the line with $R_F = 8\ \Omega$ and $s = -20\%$.

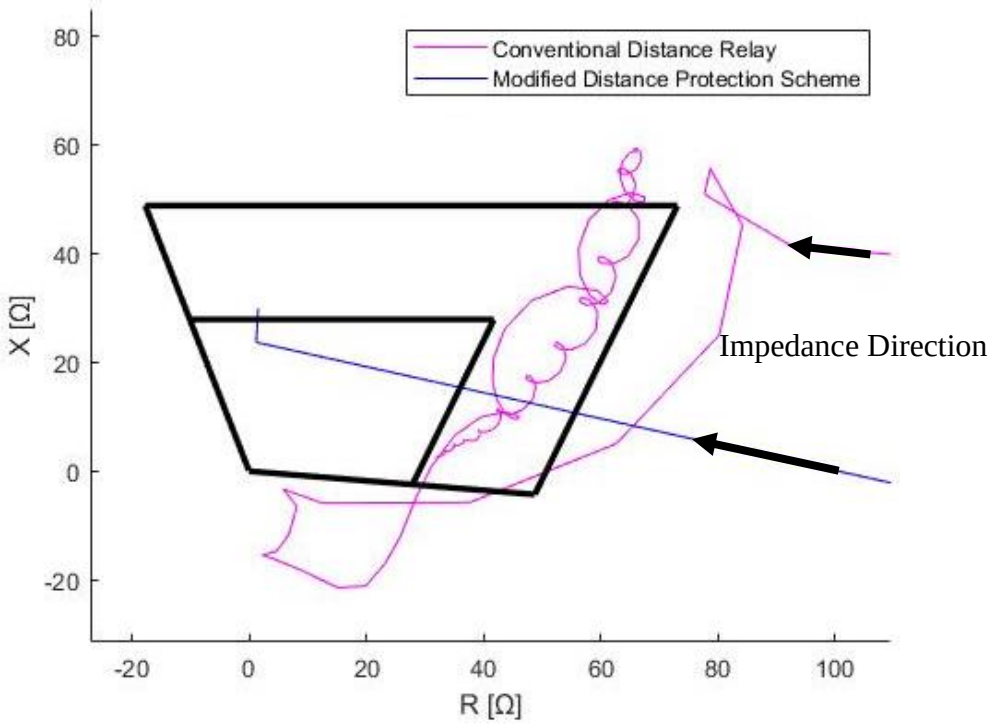

Figure 4.21 Impedance trajectory of a conventional distance relay and the modified distance protection scheme for an ABCG fault located at 80% of the line with $R_F = 8\ \Omega$ and $s = -20\%$.

For a balanced reverse fault, as shown in Figure 4.16 and discussed in section 4.4.3, none of the impedance trajectories enter the protection zone and no trip signal is generated for Relay W. Figure 4.22 shows the impedance trajectory of a conventional distance relay and the modified distance protection scheme for an ABCG reverse fault with $R_F = 8\ \Omega$ and $s = -20\%$, and neither of the impedance trajectory enters the protection zone. As a result, no trip signal is generated as expected.

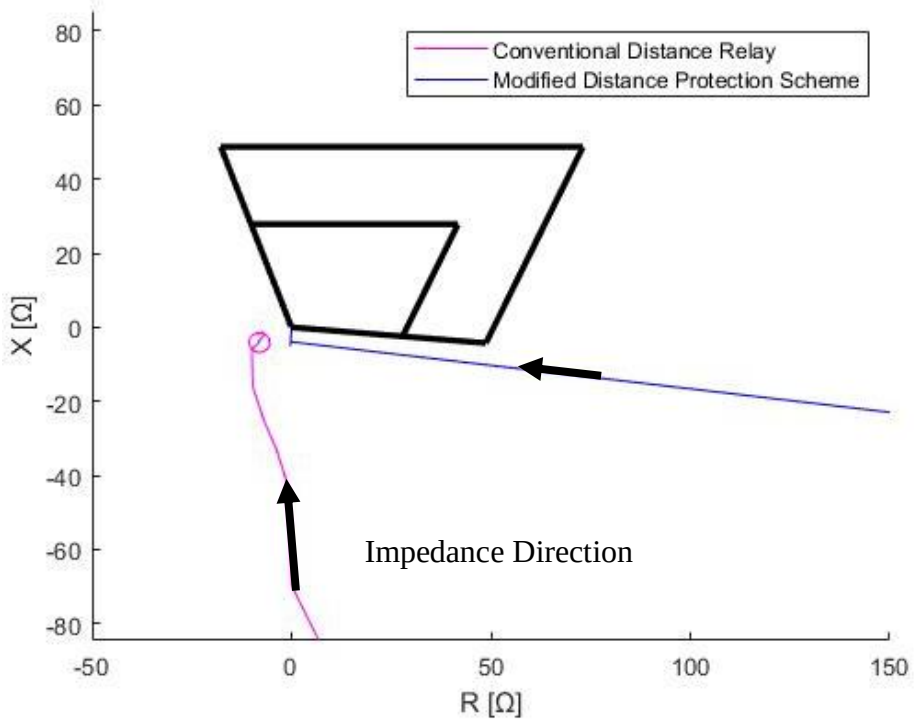

Figure 4.22 Impedance trajectory of a conventional distance relay and the modified distance protection scheme for an ABCG reverse fault with $R_F = 8\ \Omega$ and $s = -20\%$.

4.5.4 Unbalanced Faults

For unbalanced faults, since there is no frequency deviation, as discussed in section 3.3.2, Z_{actual} is calculated based on Z_m using the original phasors without the averaging filter, with the corresponding formulas as indicated in Table 4.2. The fault scenario with $s = -20\%$ and $R_F = 100\ \Omega$ for a fault located at 140% of the line (the furthest reach of the relay) is selected to evaluate the performance of the modified distance element under unbalanced faults, since this fault scenario is the one that results in the largest impedance error, as discussed in section 4.5.1.

Figure 4.23, Figure 4.24, and Figure 4.25 show the impedance trajectories of a conventional distance relay and the modified distance protection scheme for an AG, BCG, and BC fault located at 140% of the line with R_F = 100 Ω and $s = -20\%$. respectively. For unbalanced faults, as mentioned in section 4.4.3, there is no frequency deviation in the fault current, and the impedance trajectory Z_{actual} calculated using the modified distance protection scheme correctly falls at the edge of Zone 2 (140% of the line) and remains in the zones for the duration of the faults.

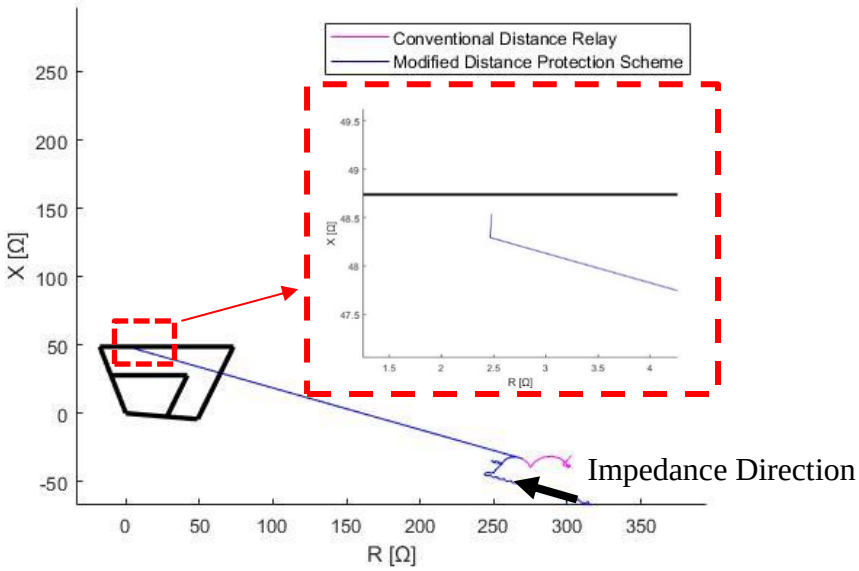

Figure 4.23 Impedance trajectory of a conventional distance relay and the modified distance protection scheme for an AG fault located at 140% of the line with $R_F = 100\ \Omega$ and $s = -20\%$.

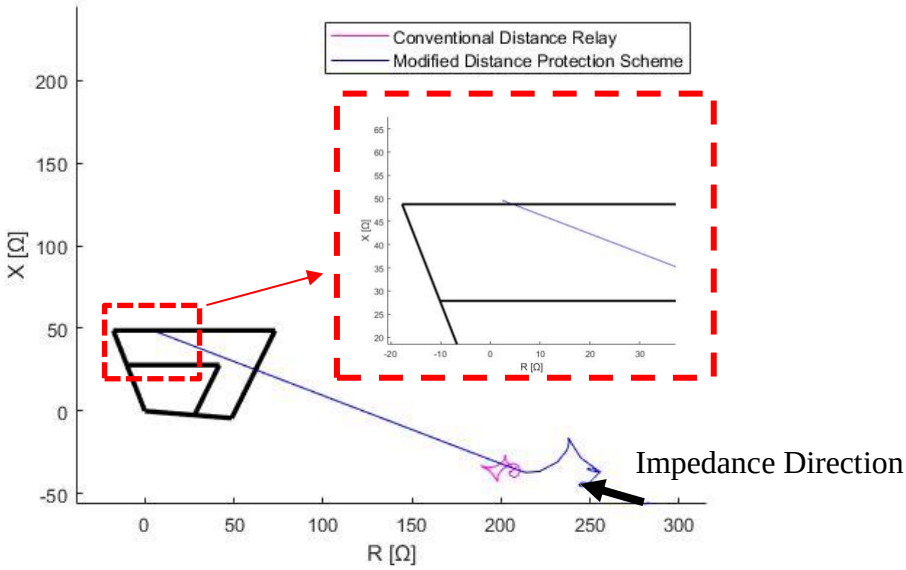

Figure 4.24 Impedance trajectory of a conventional distance relay and the modified distance protection scheme for a BCG fault located at 140% of the line with $R_F = 100\ \Omega$ and $s = -20\%$.

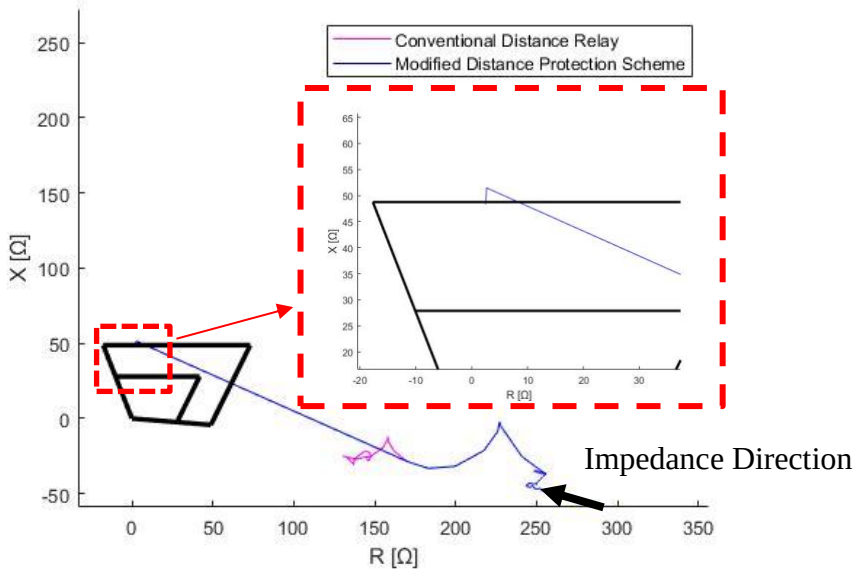

Figure 4.25 Impedance trajectory of a conventional distance relay and the modified distance protection scheme for a BC fault located at 140% of the line with $R_F = 100\ \Omega$ and $s = -20\%$.

4.6 Conclusions

This chapter presents a modified distance protection scheme to solve the protection challenges associated with conventional distance relays at the terminal of DFIG-based WTGs that are caused by the fault resistance and the frequency deviation associated with the short-circuit characteristics of the DFIG. In the presented scheme, by using an averaging filter, the phasor correction component is able to correct the current phasors, which are inaccurately calculated using the conventional DFT method. The fault resistance elimination component is able to calculate the actual impedance between the fault and relay location by removing the error term caused by a fault resistance. With the presented modified distance protection scheme, the relay located at the terminal that is close to a Type III WTG is able to correctly identify the fault location and provide zonal protection for transmission lines connected to DFIG-based wind farms.

Chapter 5
Summary and Conclusions

5.1 Summary

Power generation with RESs has experienced an accelerated increase in capacity. Most of the RESs, such as PV systems and WTGs, are connected to the grid via converters. Due to the converter characteristics, protection challenges have become more complicated and thus more sophisticated relays are required to accommodate various fault scenarios. This thesis started with a review of the various protection challenges of power systems with RESs, and then addressed two major protection challenges associated with Type III WTGs connected to transmission lines: i) the maloperation of conventional distance relays due to the frequency deviation of the current measurement caused by the short-circuit characteristics of DFIGs [15], [17]–[22]; ii) the inaccuracy of the calculated impedance between the relay and fault location due to fault resistance [23][24].

Many studies have identified the challenges associated with the protection of power systems with RESs and have proposed various algorithms to address the challenges [8]–[12], [14]–[16], [33]–[36], but only a few of them comprehensively discuss all the protection challenges within one system. Most studies use multiple small test systems to describe various protection challenges and the corresponding protection solutions [37]–[44]. In Chapter 2, a comprehensive test system was developed and used to illustrate the protection challenges of power systems with RESs and the existing solutions proposed to resolve the failure of conventional protection systems. The developed test system was utilized to discuss the protection challenges of power systems with RESs, due to the various operation modes of microgrids [8][9], changes in power system configurations [10], bidirectional current from and to the power systems [9], and various fault current levels seen by relays [11][12], and converter characteristics when RESs are connected to the power systems via converters [9][14][15][16]. Chapter 2 also used the developed system to provide a review of the existing protection schemes, which have been proposed in the literature to tackle the protection challenges associated with power systems with RESs.

Among all types of RESs, Type III WTGs are widely adopted for their advantage of variable-speed operation and reduced-size converters. However, DFIGs have a short-circuit characteristic where the frequency of the fault current deviates significantly from the rated frequency when the slip value is large [15], [17]–[22]. As a result, the phasor calculated using the conventional DFT method becomes inaccurate and result in errors within distance elements of pilot protection schemes. A modified PUTT

scheme was presented in Chapter 3 to address this issue. In addition to the conventional PUTT scheme, a frequency tracking element was used to identify the direction of the fault. With the frequency tracking elements, the modified PUTT scheme correctly prevents the maloperation of distance elements during external faults and enables the trip of the relay during internal faults.

This thesis also addressed the protection challenges associated with conventional distance relays at the terminal of DFIG-based WTGs that are caused by the fault resistance and the frequency deviation associated with the short-circuit characteristics of the DFIG. In Chapter 4, a modified distance protection scheme was developed and its performance was evaluated. The modified distance protection scheme consists of two major components: i) a phasor correction component that solves the protection challenge associated with phasor calculation error due to the off-nominal frequency of the fault current, and ii) a fault resistance elimination component that eliminates the impact of the fault resistance on the measured impedance by a conventional distance relay. Pure-fault circuits are used to calculate the pure-impedance of the WTG and pure-fault sequence networks are used to estimate the fault current flowing through the fault resistance. For faults with a large resistance, there is no off-nominal frequency component in the current measurement, and the fault resistance elimination component is able to obtain the actual impedance between the fault and relay location accurately without using the averaging filter. For faults with a small resistance where significant frequency deviation occurs in the current measurement, the averaging filter eliminates the error caused by the inaccurate phasor calculation. For faults with a fault resistance that is neither large enough to fully damp the off-nominal frequency component in the fault current, nor small enough to not impact the measured impedance, both the phasor correction method and the fault resistance component are needed to obtain the actual impedance.

Simulations were performed to evaluate the aforementioned schemes in each chapter, and both presented schemes demonstrated reliable performance in protecting transmission lines connected to WTGs.

5.2 Main Contributions

- A comprehensive test system is utilized to illustrate the protection challenges of power systems with RESs.
- A modified permissive underreaching transfer trip (PUTT) is developed to address the protection challenge associated with frequency deviation caused by the short-circuit characteristics of DFIGs.

- A modified distance protection scheme is developed to solve the protection challenges associated with conventional distance relays at the terminal of DFIG-based WTGs that are caused by the fault resistance and the frequency deviation associated with the short-circuit characteristics of the DFIG.

5.3 Future Work

Future work is recommended to:

- investigate the other protection challenges associated with other types of RESs including Type IV WTGs;
- and develop other novel protection schemes to address the protection challenges associated with other types of RESs.

Bibliography

[1] The United Nations, “United Nations Sustainable Development.” [Online]. Available: https://www.un.org/sustainabledevelopment/energy/. [Accessed: 07-Aug-2021].

[2] J. Lee and F. Zhao, “Global Wind Report | GWEC,” *Glob. Wind Energy Counc.*, p. 75, 2021.

[3] IEA, “Solar PV net capacity additions by application segment.” [Online]. Available: https://www.iea.org/data-and-statistics/charts/solar-pv-net-capacity-additions-by-application-segment-2017-2022. [Accessed: 07-Aug-2021].

[4] Environment Canada, “Powering our future with clean electricity.” [Online]. Available: https://www.canada.ca/en/services/environment/weather/climatechange/climate-action/powering-future-clean-energy.html. [Accessed: 07-Aug-2021].

[5] Canada Energy Regulator, “CER – Canada’s Renewable Power – Canada.” [Online]. Available: https://www.cer-rec.gc.ca/en/data-analysis/energy-commodities/electricity/report/canadas-renewable-power/canadas-renewable-power/provinces/renewable-power-canada-canada.html. [Accessed: 07-Aug-2021].

[6] Travers Solar, “Travers Solar.” [Online]. Available: https://www.traverssolar.com/. [Accessed: 07-Aug-2021].

[7] Beothuk Energy, “Beothuk Proposes 1GW Wind Farm off Nova Scotia - Offshore Energy.” [Online]. Available: https://www.offshore-energy.biz/beothuk-proposes-1gw-wind-farm-off-nova-scotia/. [Accessed: 07-Aug-2021].

[8] B. Bak-Jensen, M. Browne, R. Calone, R. C. Gonzalez, A. Craib, and G. Donnart, “Protection of Distribution Systems with Distributed Energy Resources,” 2015.

[9] A. Zamani *et al.*, “Microgrid Protection Systems,” 2019.

[10] A. Yazdaninejadi, A. Hamidi, S. Golshannavaz, F. Aminifar, and S. Teimourzadeh, “Impact of inverter-based DERs integration on protection, control, operation, and planning of electrical distribution grids,” *Electr. J.*, vol. 32, no. 6, pp. 43–56, 2019.

[11] M. T. Doyle, “Reviewing the impacts of distributed generation on distribution system protection,” *Proc. IEEE Power Eng. Soc. Transm. Distrib. Conf.*, vol. 1, pp. 103–105, 2002.

[12] J. Keller and B. Kroposki, “Understanding Fault Characteristics of Inverter-Based Distributed Energy Resources,” no. January, p. 48, 2010.

[13] B. Wu, Y. Lang, N. Zargari, and Samir Kouro, *Power Conversion and Control of Wind Energy Systems*. John Wiley & Sons, Inc., Hoboken, New Jersey, 2011.

[14] M. J. Reno, S. S. Venkata, W. Bower, S. Manson, J. Reilly, and G. W. Sey Jr., "Microgrid Protection : Advancing the State of the Art," no. March, 2019.

[15] Z. Shuai, C. Shen, X. Yin, X. Liu, and Z. J. Shen, "Fault Analysis of Inverter-Interfaced Distributed Generators With Different Control Schemes," *IEEE Trans. Power Deliv.*, vol. 33, no. 3, pp. 1223–1235, Jun. 2018.

[16] B. Chen, A. Shrestha, F. A. Ituzaro, and N. Fischer, "Addressing protection challenges associated with Type 3 and Type 4 wind turbine generators," *2015 68th Annu. Conf. Prot. Relay Eng. CPRE 2015*, pp. 335–344, 2015.

[17] S. Swain and P. K. Ray, "Short circuit fault analysis in a grid connected DFIG based wind energy system with active crowbar protection circuit for ridethrough capability and power quality improvement," *Int. J. Electr. Power Energy Syst.*, vol. 84, pp. 64–75, 2017.

[18] J. Morren and S. W. H. de Haan, "Short-circuit current of wind turbines with doubly fed induction generator," *IEEE Trans. Energy Convers.*, vol. 22, no. 1, pp. 174–180, 2007.

[19] F. Sulla, J. Svensson, and O. Samuelsson, "Symmetrical and unsymmetrical short-circuit current of squirrel-cage and doubly-fed induction generators," *Electr. Power Syst. Res.*, vol. 81, no. 7, pp. 1610–1618, 2011.

[20] G. Pannell, D. J. Atkinson, and B. Zahawi, "Analytical study of grid-fault response of wind turbine doubly fed induction generator," *IEEE Trans. Energy Convers.*, vol. 25, no. 4, pp. 1081–1091, 2010.

[21] B. Li, J. Liu, X. Wang, and L. Zhao, "Fault studies and distance protection of transmission lines connected to DFIG-Based wind farms," *Appl. Sci.*, vol. 8, no. 4, 2018.

[22] Nasser D. Tleis, *Power System Modeling and Fault Analysis*, vol. 53, no. 9. Oxford, U.K.: Newnes, 2008.

[23] S. H. Horowitz and A. G. Phadke, *Power System Relaying*. 2014.

[24] J. L. Blackburn and T. J. Domin, *Protective Relaying: Principles and Applications*, vol. 13, no. 5. 2015.

[25] G. Abad, J. Lopez, M. A. Rodrıguez, L. Marroyo, and G. Iwanski, *Doubly Fed Induction Machine Modeling and Control for Wind Energy Generation*. John Wiley & Sons, Inc., Hoboken, New Jersey, 2011.

[26] PSCAD, "Type-3 Wind Turbine Model (v4.5)," vol. 1, pp. 1–51, 2018.

[27] P. E. Sutherland, "Canadian grid codes and wind farm interconnections," *2015 IEEE/IAS 51st Ind. Commer. Power Syst. Tech. Conf. I CPS 2015*, pp. 3–9, 2015.

[28] IEEE Std 1159, *IEEE Recommended Practice for Monitoring Electric Power Quality*, vol. 2019. 2019.

[29] M. Hilal, Y. Errami, M. Benchagra, M. Maaroufi, M. Cherkaoui, and M. Ouassaid, "Doubly fed induction generator wind farm fault ride-through capability," *Proc. 2012 Int. Conf. Multimed. Comput. Syst. ICMCS 2012*, pp. 1079–1082, 2012.

[30] X. Zhang and S. P. Azad, "A Review of the Protection of Microgrids with Converter-Based Resources," *2020 CIGRE Canada Conf. Expo.*, 2020.

[31] The White House, "FACT SHEET: President Biden Sets 2030 Greenhouse Gas Pollution Reduction Target Aimed at Creating Good-Paying Union Jobs and Securing U.S. Leadership on Clean Energy Technologies," 2021. [Online]. Available: https://www.whitehouse.gov/briefing-room/statements-releases/2021/04/22/fact-sheet-president-biden-sets-2030-greenhouse-gas-pollution-reduction-target-aimed-at-creating-good-paying-union-jobs-and-securing-u-s-leadership-on-clean-energy-technologies/. [Accessed: 07-Aug-2021].

[32] J. Giraldez *et al.*, "Phase I Microgrid Cost Study : Data Collection and Analysis of Microgrid Costs in the United States," 2018.

[33] IEEE PES, "Impact of Inverter Based Generation on Bulk Power System Dynamics and Short-Circuit Performance," *Tech. Rep. PES-TR68*, no. July, pp. 1–71, 2018.

[34] K. Jia, Z. Yang, Y. Fang, T. Bi, and M. Sumner, "Influence of Inverter-Interfaced Renewable Energy Generators on Directional Relay and an Improved Scheme," *IEEE Trans. Power Electron.*, vol. 34, no. 12, pp. 11843–11855, 2019.

[35] J. Tang, G. Song, and C. Wang, "Adaptability analysis of directional relays in power systems with wind farms," *IET Conf. Publ.*, vol. 2016, no. CP671, 2016.

[36] B. Mahamedi and J. E. Fletcher, “Trends in the protection of inverter-based microgrids,” *IET Gener. Transm. Distrib.*, vol. 13, no. 20, pp. 4511–4522, 2019.

[37] G. Tang and R. Iravani, “Application of a Fault Current Limiter To Minimize Distributed Generation Impact on Coordinated Relay Protection,” *Int. Conf. Power Syst. Transients*, pp. 1–6, 2005.

[38] Y. Ates *et al.*, “Adaptive protection scheme for a distribution system considering grid-connected and islanded modes of operation,” *Energies*, vol. 9, no. 5, 2016.

[39] K. Dang, X. He, D. Bi, and C. Feng, “An adaptive protection method for the inverter dominated microgrid,” *2011 Int. Conf. Electr. Mach. Syst. ICEMS 2011*, pp. 1–5, 2011.

[40] A. Hooshyar and R. Iravani, “A new directional element for microgrid protection,” *IEEE Trans. Smart Grid*, vol. 9, no. 6, pp. 6862–6876, 2018.

[41] W. Chenqing, S. Guobing, and Z. Jinhua, “A novel principle of directional relay for wind power integration based on model recognition in time-domain,” *Asia-Pacific Power Energy Eng. Conf. APPEEC*, vol. 2016-Decem, pp. 1851–1855, 2016.

[42] D. Jones and K. Bennett, “Wind farm collector protection using directional overcurrent elements,” *Proc. IEEE Power Eng. Soc. Transm. Distrib. Conf.*, pp. 1–8, 2012.

[43] G. J. C. Sakis A. P. Meliopoulos, “Setting-less Protection,” pp. 1–134, 2013.

[44] E. Casagrande, W. L. Woon, H. H. Zeineldin, and D. Svetinovic, “A differential sequence component protection scheme for microgrids with inverter-based distributed generators,” *IEEE Trans. Smart Grid*, vol. 5, no. 1, pp. 29–37, 2014.

[45] IEEE PES Distribution System Analysis Subcommittee, “Distribution Test Feeders.” [Online]. Available: https://site.ieee.org/pes-testfeeders/resources/.

[46] X. Zhang and S. P. Azad, “A Modified PUTT Scheme for Transmission Lines Connecting DFIG-Based Wind Farm,” *2021 IEEE Power Energy Soc. Gen. Meet.*, 2021.

[47] X. Zhang, Y. Lu, and D. Shi, “The transient distance protection on wind farm transmission line with crowbar protection,” *2017 2nd Int. Conf. Power Renew. Energy, ICPRE 2017*, pp. 366–371, 2018.

[48] Y. Chen, M. Wen, X. Yin, Y. Cai, and J. Zheng, “Distance protection for transmission lines of

DFIG-based wind power integration system," *Int. J. Electr. Power Energy Syst.*, vol. 100, no. October 2017, pp. 438–448, 2018.

[49] S. Chen, N. Tai, C. Fan, J. Liu, and S. Hong, "Adaptive distance protection for grounded fault of lines connected with doubly-fed induction generators," *IET Gener. Transm. Distrib.*, vol. 11, no. 6, pp. 1513–1520, 2017.

[50] Z. Fan, G. Song, X. Kang, J. Tang, and X. Wang, "Three-phase fault direction identification method for outgoing transmission line of DFIG-based wind farms," *J. Mod. Power Syst. Clean Energy*, vol. 7, no. 5, pp. 1155–1164, 2019.

[51] A. Hooshyar, M. A. Azzouz, and E. F. El-Saadany, "Distance protection of lines connected to induction generator-based wind farms during balanced faults," *IEEE Trans. Sustain. Energy*, vol. 5, no. 4, pp. 1193–1203, 2014.

[52] L. Zheng, K. Jia, T. Bi, Z. Yang, and Y. Fang, "Structural Similarity Based Pilot Protection for Renewable Power Transmission Line," *IEEE Trans. Power Deliv.*, vol. 8977, no. c, 2020.

[53] J. Zare, "Protection of Transmission Lines Connected to IG-Based Wind Farms," University of Waterloo, 2020.

[54] J. Zare and S. P. Azad, "A New Relaying Scheme for Protection of Transmission Lines Connected to DFIG-based Wind Farms," pp. 1–9, 2021.

[55] A. K. Pradhan, A. Routray, and S. R. Mohanty, "A moving sum approach for fault detection of power systems," *Electr. Power Components Syst.*, vol. 34, no. 4, pp. 385–399, 2006.

[56] V. H. Makwana and B. R. Bhalja, "A New Digital Distance Relaying Scheme for Compensation of High-Resistance Faults on Transmission Line," *IEEE Trans. Power Deliv.*, vol. 27, no. 4, pp. 2133–2140, Oct. 2012.

[57] J. Ma, W. Ma, Y. Qiu, and J. S. Thorp, "An Adaptive Distance Protection Scheme Based on the Voltage Drop Equation," *IEEE Trans. Power Deliv.*, vol. 30, no. 4, pp. 1931–1940, 2015.

[58] Y. Liang, Z. Lu, W. Li, W. Zha, and Y. Huo, "A Novel fault impedance calculation method for distance protection against fault resistance," *IEEE Trans. Power Deliv.*, vol. 35, no. 1, pp. 396–407, 2020.

[59] A. K. Pradhan and G. Joós, "Adaptive distance relay setting for lines connecting wind farms," *IEEE Trans. Energy Convers.*, vol. 22, no. 1, pp. 206–213, 2007.

[60] A. Ghorbani, H. Mehrjerdi, and N. A. Al-Emadi, “Distance-differential protection of transmission lines connected to wind farms,” *Int. J. Electr. Power Energy Syst.*, vol. 89, pp. 11–18, 2017.

[61] S. Paladhi and A. K. Pradhan, “Adaptive Distance Protection for Lines Connecting Converter-Interfaced Renewable Plants,” *IEEE J. Emerg. Sel. Top. Power Electron.*, vol. 6777, no. c, pp. 1–1, 2020.

[62] S. Vejdan, M. Sanaye-Pasand, and O. P. Malik, “Accurate Dynamic Phasor Estimation Based on the Signal Model Under Off-Nominal Frequency and Oscillations,” *IEEE Trans. Smart Grid*, vol. 8, no. 2, pp. 708–719, 2017.

[63] V. S. S. Kumar, G. M. Kumar, A. S. Kumar, and D. Thukaram, “Phasor estimation at off-nominal frequencies using frequency domain interpolation,” *2017 IEEE Texas Power Energy Conf. TPEC 2017*, 2017.

[64] M. Akke and J. S. Thorp, “Sample value adjustment improves phasor estimation at off-nominal frequencies,” *IEEE Trans. Power Deliv.*, vol. 25, no. 4, pp. 2255–2263, 2010.

[65] A. G. Phadke and J. S. Thorp, “Synchronized Phasor Measurements and their Applications,” *Springer*, p. 246, 2008.

[66] A. Hooshyar, E. F. El-Saadany, and M. Sanaye-Pasand, “Fault Type Classification in Microgrids Including Photovoltaic DGs,” *IEEE Trans. Smart Grid*, vol. 7, no. 5, pp. 2218–2229, 2016.